PERGAMON

International Journal of Solids and Structures 36 (1999) 1561–1596

INTERNATIONAL JOURNAL OF SOLIDS and STRUCTURES

# Systematic description of imperfect bifurcation behavior of symmetric systems

Kiyohiro Ikeda[a,*], Kazuo Murota[b]

[a] *Department of Civil Engineering, Tohoku University, Sendai 980-8579, Japan*
[b] *Research Institute for Mathematical Sciences, Kyoto University, Kyoto 606-8502, Japan*

Received 30 April 1997; in revised form 5 February 1998

**Abstract**

A systematic method is presented for describing experimental curves of force vs strain of a system with regular polygonal (dihedral group) symmetry subject to bifurcation behavior, with an aim toward overcoming the following problems: (1) it is difficult to judge whether the system is undergoing bifurcation or not; (2) the perfect behavior of the system cannot be known due to the presence of initial imperfections; (3) those curves are often qualitatively different from bifurcation diagrams predicted by mathematics. The tools employed are: the asymptotic theory for imperfect bifurcation, such as the Koiter law, and the stochastic theory of initial imperfections. The former theory is extended in this paper to the system with regular-polygonal symmetry to present asymptotic laws for recovering perfect curves with reference to the experimental ones. These laws are formulated for physically observable displacements, instead of the variables in the mathematical bifurcation diagrams, in order to make them readily applicable to the experimental curves. The stochastic theory is combined with an asymptotic law to develop a means to identify the multiplicity of the bifurcation point. The systematic method for describing the experimental curves developed in this manner is applied to the bifurcation analysis of regular-polygonal truss domes to testify its validity. Furthermore, this method is applied to the shear behavior of cylindrical sand specimens to show that they, in fact, are undergoing bifurcation, and, in turn, to demonstrate the importance of a viewpoint of bifurcation in the study of shear behavior of materials. The need of a dual viewpoint of bifurcation and plasticity in the study of constitutive relationship of materials is emphasized to conclude the paper. 

## 1. Introduction

Bifurcation theories have been established to a high level of perfection. For bifurcation of perfect systems, Thompson and Hunt (1973) employed the elimination of passive coordinates to categorize

* Corresponding author. Tel.: 00 81(22)222-1800; fax: 00 81 22 217-7418; e-mail: ikeda@mechanics.civil.tohoku.ac.jp

0020–7683/99/$ - see front matter 
PII: S0020–7683(98)00056–0

simple critical points. The theory of plastic bifurcation was developed by Hill and Hutchinson (1975). The group-theoretic bifurcation theory is a standard procedure to describe perfect bifurcation behavior of symmetric systems, for which multiple bifurcation points appear generically (e.g., Ruelle, 1973; Sattinger, 1979; Golubitsky et al., 1988).

For bifurcation of imperfect systems, Koiter (1945) found the two-thirds power law for imperfection sensitivity to describe the influence of initial imperfections. The catastrophe theory was developed by Thom (1972), and the equivariant universal unfolding was introduced (e.g., Golubitsky et al., 1988) so as to describe the qualitative influence of initial imperfections. The notion of group-equivariance was extended to incorporate the symmetry of initial imperfections (Murota and Ikeda, 1991), and a stochastic theory of initial imperfection sensitivity was developed to describe the experimental scatter of maximum loads (Murota and Ikeda, 1992; Ikeda and Murota, 1993).

Owing to the aforementioned and other theories on bifurcation, 'analytical' or 'computational' analyses of structures and materials subject to perfect and imperfect bifurcation have been carried out in a complete and systematic manner, and led to a series of successful studies. See, e.g., Ziegler (1968), Thompson and Hunt (1973, 1984), and Ben-Haim and Elishakoff (1990) and references therein for elastic bifurcation of structures; see e.g., Hutchinson and Miles (1974), Rudnicki and Rice (1975), and Vardoulakis (1988) for plastic bifurcation of materials.

The imperfection sensitive reduction of the strength of shells observed in experiments was successfully explained by the Koiter law (1945). Yet there may still be a gap between the mathematical theory and the engineering practice in the 'experiment' of materials subject to bifurcation. Such a gap may be ascribed to the following three essential difficulties:

(1) It is difficult to judge, merely from the observed curves, whether the system under consideration is subject to bifurcation behavior or not.
(2) Experimentally observed displacements are under the influence of various kinds of initial imperfections, and the perfect system cannot be known.
(3) Observed force vs displacements can be qualitatively different from bifurcation diagrams predicted by mathematics.

Owing to the first difficulty, it is customary to ascribe the softening of force vs displacement curves of materials solely to plasticity, while it may possibly be a consequence of imperfect bifurcation, or, of the mixed presence of plasticity and bifurcation. In order to overcome the second difficulty, efforts have been made to reduce the errors in experiments. A few remarks are given below for the third difficulty. The bifurcation diagram, which is an interrelationship between an independent variable and a bifurcation parameter, is often employed in the mathematical description of bifurcation behavior. The influence of initial imperfections on this diagram in the neighborhood of a bifurcation point has fully been investigated in the foregoing references. This independent variable, however, is not necessarily related to a physically observable variable. If an observable one is employed as the abscissa of a diagram in summarizing experimental data, a resulting curve can be qualitatively different from that bifurcation diagram. Such discrepancy is often due to the geometric symmetry of a system under consideration.

In order to overcome those three difficulties, it is highly desirable to develop a strategy to eliminate or mitigate the influence of bifurcation from the experimental curves, and hence to arrive at the 'true' constitutive relationship. More specific questions to be answered in this paper are:

(1) Can we construct the curve for the perfect system with reference to a single or a number of experimental curves?
(2) Can we explain the experimental curves as imperfect bifurcation phenomena?

Clues to answer these questions have already been cited above, that is, the Koiter law and the stochastic theory of initial imperfection sensitivity. In this paper, we generalize the Koiter law, which yields information only on the limit point of an imperfect curve, to arrive at asymptotic laws on imperfection sensitivity that can offer information on the whole curve. The extension is made with respect to the following three aspects:

(1) applicability to experimentally observable displacements,
(2) the robustness against experimental errors, and
(3) applicability to double bifurcation points.

The implementation of the first and the second aspects, which are mandatory in the application to experimental curves, is performed through the refinement of a series of references: Ikeda and Goto (1993) and Ikeda et al. (1997a, b). The implementation of the third aspect is necessitated in dealing with symmetric systems, such as, dome structures, cylindrical soil or concrete specimens. This is based on Murota and Ikeda (1991).

Through a combination of 'the asymptotic laws' extended in this manner with the 'stochastic theory of imperfection sensitivity', we present a systematic procedure to describe imperfect bifurcation behavior of a system with regular-polygonal (dihedral group) symmetry. The bifurcation equation is derived by means of a standard procedure of the elimination of passive coordinates, or, the Liapunov-Schmidt reduction, exploiting the dihedral group symmetry. Then the independent variable(s) of this equation is transformed into a physically observable displacement, which is classified into two types: that with symmetry and that without it. For each type of displacement, the explicit form of a force vs displacement curve and a pertinent power law are derived. In particular, a power law for a physically observable displacement for double eigenvalues serves as an essential contribution of this paper. A combination of the stochastic method and the generalized Koiter law is presented as a means to identify the multiplicity of a bifurcation point. As a result of these, we present a systematic strategy to recover the curve of an imperfect system, and hence to judge if the bifurcation is actually taking place or not. This strategy is applied to the numerical analyses of regular-polygonal truss domes to testify its validity. Furthermore, it is applied to the shear behavior of cylindrical sand specimens to reveal that they, in fact, are undergoing bifurcation, and, in turn, to demonstrate the importance of a viewpoint of bifurcation in the future study of the shear behavior of materials.

## 2. Imperfection sensitivity laws

A series of imperfection sensitivity laws for describing experimental force vs displacement curves subject to imperfect bifurcation behavior are introduced through the extension and reorganization of the results of Ikeda et al. (1997b) to a system with regular-polygonal symmetry.

### 2.1. Formulation

We consider a system of nonlinear equilibrium equations

$$\mathbf{F}(\mathbf{u}, f, \mathbf{v}) = \mathbf{0}, \tag{1}$$

where $\mathbf{u} \in \mathbf{R}^N$ is a displacement (or position) vector, $f \in \mathbf{R}$ a loading parameter, $\mathbf{v} \in \mathbf{R}^p$ an imperfection parameter vector, $\mathbf{F}$ a sufficiently smooth (e.g., analytic) nonlinear function in $\mathbf{u}$, $f$, and $\mathbf{v}$; $N$ is the number of degrees of freedom and $p$ the number of imperfection parameters.

For a fixed $\mathbf{v}$, the solutions $(\mathbf{u}, f)$ of the above system of equations make up equilibrium paths. Let $(\mathbf{u}_c, f_c) = (\mathbf{u}_c(\mathbf{v}), f_c(\mathbf{v}))$ denote a critical point of the system described by $\mathbf{v}$ (the subscript $(\cdot)_c$ refers to the critical point). The Jacobian (tangent stiffness) matrix $J = \partial\mathbf{F}/\partial\mathbf{u}$ is singular at $(\mathbf{u}_c, f_c)$ and, in particular, at the critical point $(\mathbf{u}_c^0, f_c^0) = (\mathbf{u}_c(\mathbf{v}^0), f_c(\mathbf{v}^0))$ of the perfect system. Here the superscript $(\cdot)^0$ refers to the perfect system described by $\mathbf{v} = \mathbf{v}^0$. We put

$$\begin{aligned} &\mathbf{u} = \mathbf{u}_c^0 + \tilde{\mathbf{u}}, \quad \mathbf{u}_c = \mathbf{u}_c^0 + \tilde{\mathbf{u}}_c, \\ &f = f_c^0 + \tilde{f}, \quad f_c = f_c^0 + \tilde{f}_c, \end{aligned} \tag{2}$$

where $\tilde{\mathbf{u}}$ and $\tilde{\mathbf{u}}_c$ mean the increments of the displacement and the critical displacement, respectively, from $\mathbf{u}_c^0$ for the critical point of the perfect system, and $\tilde{f}$ and $\tilde{f}_c$ the increments of the load and the critical load, respectively. To distinguish the mode and the magnitude of an imperfection, we write

$$\mathbf{v} = \mathbf{v}^0 + \varepsilon\mathbf{d} \tag{3}$$

with a scalar nonnegative parameter $\varepsilon$ and an imperfection mode vector $\mathbf{d} \in \mathbf{R}^p$.

By imperfection sensitivity we mean the dependence of relevant quantities, such as $\tilde{f}_c$, on $\varepsilon$ and/or $\mathbf{d}$. Most of the arguments of this paper are asymptotic in the sense that they are valid only when $\varepsilon$ is sufficiently small.

### 2.2. Koiter's two-thirds power law

For an unstable, simple, symmetric (pitchfork-type) point $(\mathbf{u}_c^0, f_c^0)$ of bifurcation, the system (1) of equations can be reduced to a single bifurcation equation

$$A_{110} w\tilde{f} + A_{300} w^3 + A_{001}\varepsilon + \text{h.o.t.} = 0 \tag{4}$$

in a single variable $w \in \mathbf{R}$, where h.o.t. means a higher order term that can be ignored as $\varepsilon$ tends to zero, and $A_{110}$, $A_{300}$, and $A_{001}$ are constants ($A_{001}$ depends on the imperfection mode $\mathbf{d}$). This equation is valid in the vicinity of the bifurcation point $(\mathbf{u}_c^0, f_c^0)$, that is, $(w, \tilde{f}, \varepsilon) = (0, 0, 0)$ for sufficiently small $\varepsilon$. Because this point is assumed to be unstable, we have $A_{110}A_{300} > 0$ for this case.

The imperfect system described by eqn (4) with $\varepsilon \neq 0$ has a limit point, as depicted in Fig. 1, and the location $(w_c, \tilde{f}_c)$ of this limit point is calculated as

$$w_c = \left(\frac{A_{001}}{2A_{300}}\right)^{1/3} \varepsilon^{1/3} + \text{h.o.t.}, \tag{5}$$

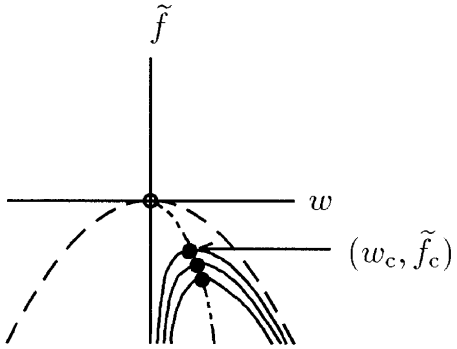


Fig. 1. Koiter's two-thirds power law and the asymptotic relation (7). (—) denotes a curve for an imperfect system, (- - -) indicates that for the perfect one, (– - - –) indicates the parabola (7), (○) stands for the bifurcation point of the perfect one, and (●) for a limit point of an imperfect one.

$$\tilde{f}_c = -\beta\varepsilon^{2/3} + \text{h.o.t.}, \quad \beta = \frac{3A_{300}^{1/3}A_{001}^{2/3}}{2^{2/3}A_{110}}, \tag{6}$$

where $\beta$ is a constant independent of $\varepsilon$. Equation (6) is the famous Koiter's two-thirds power law, which serves as a prototype of imperfection sensitivity laws.

On eliminating $\varepsilon$ from eqns (5) and (6), we obtain an asymptotic relation

$$\tilde{f}_c + g_K w_c^2 = 0 \tag{7}$$

with $g_K = 3A_{300}/A_{110} > 0$. It is important that $g_K$ is a constant independent of the imperfection mode **d**, whereas $A_{001}$ does depend on **d**. The relation (7) is illustrated in Fig. 1 by a series of (·) threaded with a dotted–dashed line. This relation (7) can potentially be useful for a treatment of imperfection sensitive bifurcation behavior, but in its present form it suffers from serious drawbacks:

(1) The variable $w$ is more mathematical than it is physical, and as a consequence, the critical displacement $w_c$ is not always observed (or observable) in experiments. Note that the variable $w$ is introduced in the course of mathematical reduction to obtain the bifurcation equation. It is not an $f$ vs $w$ curve but an $f$ vs $u_{i^*}$ one (with a particular $i^*$) that is to be acquired in customary experiments.
(2) Even if the variable $w$ is observed, the value of $w_c$ must be determined by identifying the limit point of an observed equilibrium path, which is necessarily blurred due to various noises and errors in numerical analyses and physical experiments. In such situations the values of $w_c$, being the abscissa of the limit point, cannot be determined in a reliable manner, whereas the value of $f_c$, the ordinate of the limit point, is relatively easy to determine.

### 2.3. Generalized imperfection sensitivity law

Generalizing the relation (7) for the Koiter law, we consider a parabola

$$\tilde{f} + gw^2 = 0 \tag{8}$$

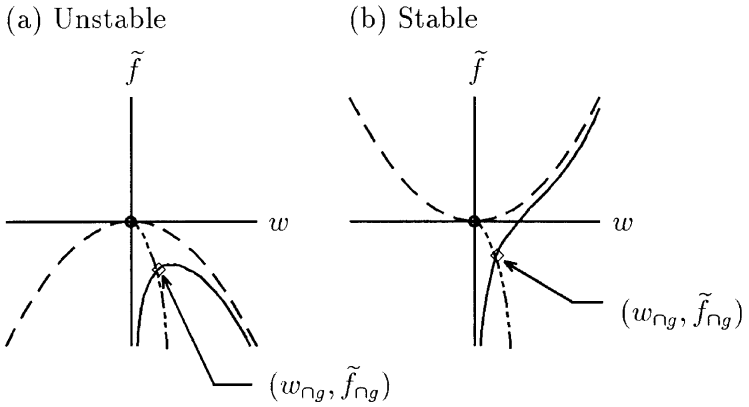


Fig. 2. Generalization of the Koiter law and the parabola (8). (a) Unstable, simple, symmetric bifurcation point. (b) Stable, simple, symmetric bifurcation point. (—) denotes a curve for an imperfect system, (- - -) indicates that for the perfect one, the dotted–dashed one (– · – · –) stands for the parabola (8), (○) for the bifurcation point of the perfect one, and (◇) for the intersection point of the parabola and an imperfect path.

with an arbitrary constant $g$ shown by the dotted–dashed line in Fig. 2, and its intersection point $(w_{\cap g}, \tilde{f}_{\cap g})$ with the imperfect path, shown by (◇). The substitution of eqn (8) for the parabola into the bifurcation eqn (4) yields

$$w_{\cap g} = \left(\frac{A_{001}}{gA_{110} - A_{300}}\right)^{1/3} \varepsilon^{1/3} + \text{h.o.t.} \tag{9}$$

The combination of this expression with eqn (6) for $\tilde{f}_c$ yields

$$\tilde{f}_c = -\frac{3A_{300}^{1/3}(gA_{110} - A_{300})^{2/3}}{2^{2/3}A_{110}}(w_{\cap g})^2 + \text{h.o.t.}, \tag{10}$$

which shows that $\tilde{f}_c$ is proportional to $(w_{\cap g})^2$ asymptotically as $\varepsilon \to 0$. Note that the coefficient of proporitonality, being independent of $A_{001}$, is a constant independent of the imperfection mode **d**, while it is remarked in this connection that the coefficient $\beta$ in eqn (6) depends on **d**.

The expression (10) gives an asymptotic relation between coordinates of two distinct points, namely, the ordinate $\tilde{f}_c$ of the limit point $(w_c, \tilde{f}_c)$ of an imperfect system and the abscissa $w_{\cap g}$ of the intersection point $(w_{\cap g}, \tilde{f}_{\cap g})$. The asymptotic law (10) has an advantage that $w_{\cap g}$ can be determined much more reliably than $w_c$. Thus, the introduction of the general parabola (8) resolves the second drawback of the original relation (7) of the Koiter law mentioned at the end of Section 2.2. The law (10) has another advantage over the original relation (7). As can be seen from Fig. 2, the intersection point exists both for stable- and unstable-symmetric bifurcation points, and hence the generalized law (10) is applicable to both types of points, whereas the Koiter law yields physically meaningful information only for an unstable point of bifurcation.

Next, we address the first problem with eqn (7) of the Koiter law concerning the observability of $w_c$ in the experiment, and shall further improve the asymptotic law (10). Namely, we aim at an

asymptotic law, as well as the bifurcation equation, expressed in terms of an observable variable $u_{i^*}$ with a particular $i^*$.

With reference to the bifurcation point $(\mathbf{u}_c^0, f_c^0)$, we choose a set of $N$ (orthonormal) vectors $\{\boldsymbol{\eta}_i \mid i = 1, \ldots, N\}$ such that

$$J^0\boldsymbol{\eta}_1 = \mathbf{o}; \quad J^0\boldsymbol{\eta}_i \neq \mathbf{o}, \quad i = 2, \ldots, N,$$

that is, $\boldsymbol{\eta}_1$ corresponds to the critical eigenvector of the Jacobian matrix $J^0 = J(\mathbf{u}_c^0, f_c^0, \mathbf{v}^0)$ at $(\mathbf{u}_c^0, f_c^0)$ for $\mathbf{v} = \mathbf{v}^0$. We express the displacement $\mathbf{u}$ as

$$\mathbf{u} = \mathbf{u}_c^0 + \sum_{j=1}^{N} w_j\boldsymbol{\eta}_j$$

in terms of incremental variables $(w_j \mid j = 1, \ldots, N)$.

By a standard procedure called the 'elimination of passive coordinates', or, the Liapunov–Schmidt reduction (see the Appendix), we can obtain the bifurcation eqn (4) for the variable $w = w_1$:

$$\hat{F}_1(w, \tilde{f}, \varepsilon) = A_{110}w\tilde{f} + A_{300}w^3 + A_{001}\varepsilon + \text{h.o.t.} = 0, \tag{11}$$

and the remaining equations for the passive coordinates $w_i$ $(i = 2, \ldots, N)$:

$$\hat{F}_i(\mathbf{w}, \tilde{f}, \varepsilon) = e_i w_i + a_i\tilde{f} + b_i\varepsilon + c_i w^2 + \text{h.o.t.} = 0, \tag{12}$$

where $A_{ijk}$'s are coefficients, $e_i$ is the $i$th eigenvalue of $J^0$ and $a_i$, $b_i$ and $c_i$ are constants. It turns out that

$$w = O(\varepsilon^{1/3}); \quad w_i = O(\varepsilon^{2/3}), \quad i = 2, \ldots, N; \quad \tilde{f} = O(\varepsilon^{2/3})$$

($O(\cdot)$ denotes the order of the term therein).

In order to arrive at an explicit form of the $f$ vs $u_{i^*}$ curve, we express $\tilde{u}_{i^*} \equiv u_{i^*} - (u_{i^*})_c^0$ with a particular $i = i^*$ in terms of $w$ and $\tilde{f}$ through the substitution of eqn (12) for the passive coordinates into eqn (11), that is,

$$\tilde{u}_{i^*} = \sum_{j=1}^{N} \eta_{i^*j} w_j = \eta_{i^*1} w + r_{i^*}\tilde{f} + s_{i^*}w^2 + \text{h.o.t.}, \tag{13}$$

where the term of $\varepsilon$ in eqn (12) has been omitted in this equation as it is a higher order term; $\eta_{i^*j}$ is the $i^*$th component of $\boldsymbol{\eta}_j = (\eta_{1j}, \ldots, \eta_{Nj})^T$; and

$$r_{i^*} = -\sum_{j=2}^{N} \frac{\eta_{i^*j}a_j}{e_j}, \quad s_{i^*} = -\sum_{j=2}^{N} \frac{\eta_{i^*j}c_j}{e_j}$$

are some constants. We write $\tilde{u} = \tilde{u}_{i^*}$, $r = r_{i^*}$ and $s = s_{i^*}$ for brevity.

As can be seen from eqn (13), the properties of $\tilde{u}$ can be categorized with reference to the vanishing and non-vanishing of the coefficient $\eta_{i^*1}$ of $w$, that is,

$$\begin{cases} \tilde{u} = O(w) & \text{if } \eta_{i^*1} \neq 0, \\ \tilde{u} = O(w^2) & \text{if } \eta_{i^*1} = 0. \end{cases} \tag{14}$$

The latter case ($\eta_{i^*1} = 0$) can occur not only by an accidental numerical cancellation but also generically as a consequence of group symmetry, if the displacement $u_{i^*}$ is invariant under the geometric transformation that corresponds to $w \to -w$ (see Section 2.4 and the Appendix). In fact, this case often takes place in experiments, and hence is a primary concern of this paper.

*2.3.1. Displacement* $u_{i^*}$ *without symmetry* ($\eta_{i^*1} \neq 0$)

For a general displacement $u_{i^*}$ without particular symmetry ($\eta_{i^*1} \neq 0$), our preliminary considerations leading to the asymptotic law (10) need only marginal modifications. Equation (13) is solved for $w$ as

$$w = \frac{1}{\eta_{i^*1}}\left(\tilde{u} - \frac{\tilde{f}}{E}\right) + \text{h.o.t.} \tag{15}$$

The substitution of eqn (15) into eqn (11) yields the asymptotic expression

$$\left(\tilde{u} - \frac{\tilde{f}}{E}\right)\tilde{f} + p^*\left(\tilde{u} - \frac{\tilde{f}}{E}\right)^3 + q^*\varepsilon + \text{h.o.t.} = 0, \tag{16}$$

for the curve of an imperfect system, where

$$p^* = \frac{A_{300}}{\eta_{i^*1}^2 A_{110}}, \quad q^* = \frac{\eta_{i^*1} A_{001}}{A_{110}}.$$

Note that $p^*$ is a constant associated with the curvature of the bifurcation path and $q^*$ is a scaling factor, depending on the imperfection mode **d**, of the magnitude $\varepsilon$ of the initial imperfection. General views of the perfect and imperfect paths expressed by eqn (16) are depicted in Fig. 3(a).

Instead of the parabola (8) in the $(w,\tilde{f})$-plane, we consider a parabola

$$\tilde{f} + g\tilde{u}^2 = 0 \tag{17}$$

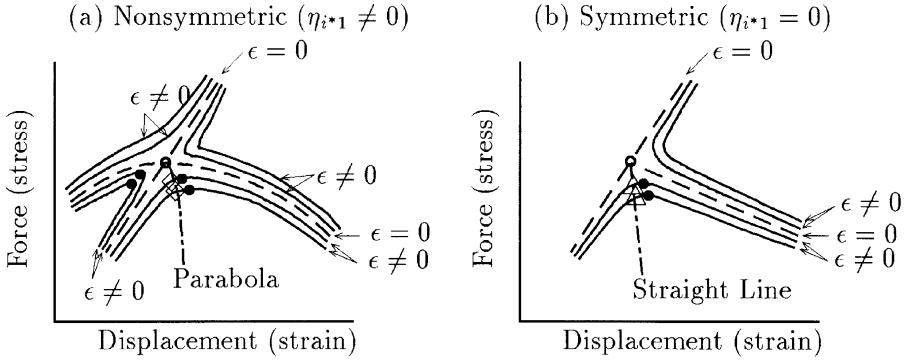


Fig. 3. General views of force vs displacement curves in the vicinity of an unstable, simple, symmetric bifurcation point. (a) Nonsymmetric (non-$D_n$-invariant) displacement with $\eta_{i^*1} \neq 0$. (b) Symmetric ($D_n$-invariant) displacement with $\eta_{i^*1} = 0$. (—) denotes a curve for an imperfect system, (- - -) indicates that for the perfect one, (○) is the bifurcation point of the perfect one, (●) is a limit point of an imperfect one, (◇) is the intersection point of the straight line with an imperfect one, and (△) that of the parabola with an imperfect one.

in the $(\tilde{u},\tilde{f})$-plane (where $g$ is a constant), shown by the dotted–dashed line in Fig. 3(a) and its intersection point $(\tilde{u}_{\cap g}, \tilde{f}_{\cap g})$, shown as $(\diamond)$, with the imperfect $\tilde{f}$ vs $\tilde{u}$ curve. The substituting of eqn (17) into eqn (16) and the omitting of higher order terms lead to

$$\tilde{u}\cap g = \left(\frac{q^*}{g-p^*}\right)^{1/3} \varepsilon^{1/3} + \text{h.o.t.} = \left(\frac{\eta_{i^*1}^3 A_{001}}{g\eta_{i^*1}^2 A_{110} - A_{300}}\right)^{1/3} \varepsilon^{1/3} + \text{h.o.t.} \tag{18}$$

The eliminating of $\varepsilon$ from eqn (18) and the Koiter law (6) yields a power law

$$\begin{aligned}\tilde{f}_c &= -\frac{3(p^*)^{1/3}(g-p^*)^{2/3}}{2^{2/3}}(\tilde{u}\cap g)^2 + \text{h.o.t.} \\ &= -\frac{3A_{300}^{1/3}(g\tilde{A}_{110} - A_{300})^{2/3}}{2^{2/3}\tilde{A}_{110}}(\tilde{u}\cap g)^2 + \text{h.o.t.},\end{aligned} \tag{19}$$

where $\tilde{A}_{110} = \eta_{i^*} A_{110}$. As expected, the law (19) is qualitatively identical with eqn (10).

*2.3.2. Displacement* $\mathrm{u}_{i^*}$ *with symmetry* $(\eta_{i^*1} = 0)$

For a symmetric displacement $u_{i^*}$ with $\eta_{i^*1} = 0$, the asymptotic relation (10) and the bifurcation eqn (11) take qualitatively different forms. Equation (13) becomes:

$$\tilde{u} = r\tilde{f} + sw^2 + \text{h.o.t.} \tag{20}$$

On eliminating $w$ from eqns (11) and (20), we obtain

$$\sqrt{\text{sign}(s)\left(\tilde{u} - \frac{\tilde{f}}{E}\right)}\left[\tilde{f} + p\left(\tilde{u} - \frac{\tilde{f}}{E}\right)\right] \pm q\varepsilon + \text{h.o.t.} = 0, \tag{21}$$

with an inequality condition

$$\text{sign}(s)\left(\tilde{u} - \frac{\tilde{f}}{E}\right) \geqslant 0. \tag{22}$$

Here sign $(s)$ denotes the sign of $s$ and $E = 1/r$ denotes the tangent of the main path for the perfect system $(\varepsilon = 0)$, which is associated with the trivial solution $w = 0$, and $p$ and $q$ are parameters, being defined as:

$$p = \frac{A_{300}}{sA_{110}}, \quad q = \frac{A_{001}|s|^{1/2}}{A_{110}}. \tag{23}$$

With this notation, the Koiter law (6) is written as

$$\tilde{f}_c = -\text{sign}(s)\frac{3_p{}^{1/3}q^{2/3}}{2^{2/3}}\varepsilon^{2/3} + \text{h.o.t.} \tag{24}$$

By putting $\varepsilon = 0$ in eqn (21) we obtain

$$\begin{cases} \tilde{u}-\dfrac{\tilde{f}}{E}+\text{h.o.t}=0 & \text{on main path,} \\ \tilde{f}+p\left(\tilde{u}-\dfrac{\tilde{f}}{E}\right)+\text{h.o.t.}=0, \quad \text{sign}(s)\left(\tilde{u}-\dfrac{\tilde{f}}{E}\right)\geqslant 0 & \text{on bifurcation path,} \end{cases} \tag{25}$$

for the equilibrium of the perfect system. Owing to the inequality condition, the bifurcation path expressed by eqn (25) branches toward only one direction from the bifurcation point. This is a qualitative change from the pitchfork-type diagram.

For an imperfect system, it should be remarked that the inequality condition (22) indicates that all imperfect paths exist only on one side of the main path; the side depends on the sign of $s$. For a specified value of $\varepsilon$, $\pm$ in eqn (21) corresponds to a pair of imperfect paths; $+$ is associated with a path above the bifurcation path and $-$ with another path below it, or, vice versa [cf Fig. 3(b)].

Instead of a parabola we now consider a straight line

$$\tilde{f}+h\tilde{u}=0 \tag{26}$$

(where $h$ is a constant) shown by the dashed-and-dotted line in Fig. 3(b), and its intersection point $(\tilde{u}_{|h},\tilde{f}_{|h})$, as shown as ($\triangle$), with the imperfect $\tilde{f}$ vs $\tilde{u}$ curve. A substitution of eqn (26) of the straight line into eqn (21) results in

$$\tilde{u}_{|h}=\gamma\varepsilon^{2/3}+\text{h.o.t.}, \tag{27}$$

where

$$\gamma=\frac{q^{2/3}}{\text{sign}(s)\left(1+\dfrac{h}{E}\right)^{1/3}\left[-h+p\left(1+\dfrac{h}{E}\right)\right]^{2/3}}.$$

The elimination of the imperfection magnitude $\varepsilon$ from the Koiter law (24) and the expression (27) leads to a generalized asymptotic law

$$\tilde{f}_{\text{c}}=-\gamma^{*}\tilde{u}_{|h}+\text{h.o.t.} \tag{28}$$

with

$$\gamma^{*}=\frac{3}{2^{2/3}}\left[p\left(1+\frac{h}{E}\right)\right]^{1/3}\left[-h+p\left(1+\frac{h}{E}\right)\right]^{2/3}. \tag{29}$$

This denotes a linear relationship between a pair of physically observable variables $\tilde{u}_{|h}$ and $\tilde{f}_{\text{c}}$ that passes the origin $(\tilde{u}_{|h},\tilde{f}_{\text{c}})=(0,0)$. Namely, $(\tilde{u}_{|h},\tilde{f}_{\text{c}})$ for different values of $\varepsilon$ all lie on the line (28) with a common slope $-\gamma^{*}$. It is emphasized that the coefficient $\gamma^{*}$ is independent of the imperfection mode **d**, whereas $\gamma$ is not.

### *2.4. Extension to systems of regular-polygonal symmetry*

In this subsection, we present the outline of the bifurcation of a system with the dihedral group symmetry, and the applicability of the asymptotic laws presented in Sections 2.2 and 2.3 to this system, whereas details are worked out in the Appendix.

Qualitative aspects of bifurcation of symmetric systems have successfully been described by a standard strategy, called the group-theoretic bifurcation theory (see, e.g., Sattinger, 1979; Golubitsky and Stewart, 1986; Golubitsky et al., 1988). The symmetry of the system under consideration is formulated as the equivariance to a group $G$. The symmetry of a bifurcated solution is characterized by a subgroup $G_1$ of $G$. Namely, the symmetry of the solution is reduced at the onset of bifurcation, which is characterized by the change in symmetry: $G \to G_1$.

To describe the symmetry of a regular-polygonal symmetry, we set the group $G$ to be the dihedral group $\mathrm{D}_n$ of degree $n$ defined by

$$\mathrm{D}_n = \{c(2\pi k/n), \sigma c(2\pi k/n) \mid k = 0, 1, \ldots, n-1\}$$

with $c(2\pi) = \sigma^2 = (\sigma c(\pi))^2 = e$. Here $e$ denotes the unit transformation, $c(\theta)$ represents a rotation around the $Z$-axis through an angle of $\theta$, and $\sigma$ represents a reflection with respect to the $YZ$-plane. The subgroups of $\mathrm{D}_n$ are enumerated by

$$\{\mathrm{D}^j_m \mid j = 1, \ldots, n/m; m \text{ divides } n\} \quad \text{and} \quad \{\mathrm{C}_m \mid m \text{ divides } n\},$$

where

$$\mathrm{D}^j_m = \{c(2\pi k/m), \sigma c(2\pi[(j-1)/n + k/m]) \mid k = 0, 1, \ldots, m-1\};$$
$$\mathrm{C}_m = \{c(2\pi k/m) \mid k = 0, 1, \ldots, m-1\}. \tag{30}$$

The bifurcation of a system with the dihedral group symmetry has been studied extensively (e.g., Fujii et al., 1982; Golubitsky and Stewart, 1986; Golubitsky et al., 1988; Buzano et al., 1988; Healey, 1988; Ikeda et al., 1991; Gatermann, 1993). We consider the bifurcation points on the fundamental equilibrium path of a $\mathrm{D}_n$- symmetric system that are generically either simple or double point of bifurcation according to whether the dimension of the kernel of the Jacobian $J^0_c$ is equal to one or two.

### 2.4.1. Simple bifurcation point

At a simple bifurcation point, the symmetry of the critical eigenvector for the kernel of the Jacobian $J^0_c$ is labeled by: $\mathrm{C}_n$, $\mathrm{D}_{n/2}$ or $\mathrm{D}^2_{n/2}$. In each case, the bifurcation equation is expressed as the form of eqn (11) and the remaining equations as the form of eqn (12). All the formulas presented in Sections 2.2 and 2.3 are applicable to a simple bifurcation point of a $\mathrm{D}_n$-symmetric system. The symmetry of an observed variable $u_{i*}$, to be precise, can be characterized by $\mathrm{D}_n$-invariance of $u_{i*}$.

### 2.4.2. Double bifurcation point

Double bifurcation points on a $\mathrm{D}_n$-symmetric fundamental path can be further classified in view of the symmetry of a pair of critical eigenvectors of $J^0_c$. At a double bifurcation point, these vectors are both $\mathrm{C}_m$-symmetric (though an appropriate superposition of these vectors can be $\mathrm{D}^j_m$-symmetric), where $m$ is an integer that divides $n$ and satisfies $n/m \geqslant 3$. We call $\hat{n} = n/m$ the 'index' of the double point. The index $\hat{n}$ is indeed an important parameter in that it characterizes the laws for imperfection sensitivity as follows (cf Murota and Ikeda, 1992):

$$\tilde{f}_c \sim \begin{cases} C(\psi)|a|^{1/2}\varepsilon^{1/2} & \text{if } \hat{n}=3, \\ C(\psi)|a|^{2/3}\varepsilon^{2/3} & \text{if } \hat{n}=4, \\ C_0|a|^{2/3}\varepsilon^{2/3} & \text{if } \hat{n}\geqslant 5, \end{cases}$$

where $a = a(\mathbf{d}) = |a|\exp(i\psi)$ is a complex variable expressing the influence of imperfection pattern vector $\mathbf{d}$ and $C_0$ is a constant independent of $\mathbf{d}$. The index $\hat{n}$ also characterizes the explicit form of the equilibrium path of an imperfect system.

If $\hat{n} \geqslant 5$, the equilibrium path of an imperfect system can be represented by

$$r\tilde{f} + r^3 - |a|\varepsilon = 0 \tag{31}$$

in terms of $r = \sqrt{w_1^2 + w_2^2}$, where $(w_1, w_2)$ is the orthonormal coordinates of the two-dimensional kernel space of $J^0$. Moreover, for a $D_n$-invariant displacement $u_{i^*}$, the increment $\tilde{u} \equiv u_{i^*} - (u_{i^*})_c^0$ is expressed as

$$\tilde{u} = R_{i^*}\tilde{f} + S_{i^*}r^2 + \text{h.o.t.}, \tag{32}$$

where $R_{i^*}$ and $S_{i^*}$ are constants. Note that eqn (32) is exactly of the same form as eqn (20) for a symmetric displacement of a simple, symmetric bifurcation point with $\eta_{i^*1} = 0$. In addition, recall that the bifurcation eqn (31) is of the same form as eqn (11) for the simple point. As a consequence of these, all the results presented in Section 2.3.2 for a symmetric displacement for a simple point apply to a symmetric one for a double point with $\hat{n} \geqslant 5$ as well. In particular, a straight line $\tilde{f} + h\tilde{u} = 0$ should be employed and then a linear relationship (28) between $\tilde{u}_{|h}$ and $\tilde{f}_c$ holds good asymptotically. It should be emphasized here that when $\hat{n} = 3$ or 4, or when $u_{i^*}$ is not $D_n$-invariant, these results are not applicable.

## 3. Recovering perfect systems from imperfect system behaviors

As was mentioned in the introduction, a difficulty in the interpretation of experimental curves subject to bifurcation behavior lies in the fact that the curve for the perfect system is unknown. In order to resolve this difficulty, a systematic procedure is presented in this section for recovering the perfect curve with reference to experimental curves. We assume the presence of a unique perfect system and its unique bifurcation point. We further assume the absence of the mode switching behavior and recursive bifurcation behavior among a few bifurcation modes. See Ikeda and Murota (1997) and Ikeda et al. (1997b) for a systematic procedure to sort out these behaviors.

At the first step of the recovering of the perfect curve, the symmetry of the displacement $u = u_{i^*}$ under consideration is to be investigated. For a displacement without symmetry, the formulas in Section 2.3.1 are to be employed, while for a symmetric displacement are those in Section 2.3.2. We focus on the symmetric displacement in the remainder of this section in presenting a procedure for recovering the perfect behavior, whereas a procedure of that without symmetry can be obtained simply by replacing relevant formulas. It should be emphasized here that for such a symmetric displacement the formulas for a simple, symmetric bifurcation point and those for a double one are identical.

### 3.1. Recovery from a single imperfect path

The values of the parameters needed in recovering the perfect curve in the plane of $(u,f)$ consist of the location $(u_c^0,f_c^0)$ of the bifurcation point and the parameters $p$ and $E$ in eqn (25), whereas the values of $q\varepsilon$ in eqn (21) is needed in the simulation of the experimental (imperfect) curve. The information to be extracted from a single experimental curve is the location $\tilde{u}_{|h}$ of the intersection point of the straight line (26) with the experimental curve for different values of $h$, where the 'origin' $(u_c^0,f_c^0)$ is unknown. This is based on the fact that the law (28) holds for any values of $h$, say $(h_i \mid i = 1,2,\ldots)$.

Among other possibilities, the following procedure may be suggested. Assume the location $(u_c^0,f_c^0)$ of the bifurcation point. If we employ four different values of $h$ say $(h_i \mid i = 1,2,3,4)$, we can estimate $p$ and $E$ on the basis of eqn (28) with eqn (29) from the observed values of $\tilde{u}_{|h}$. To be concrete, for two different values $h_i$ and $h_j$, eqn (28) with eqn (29) yields

$$\left(\frac{\tilde{u}_{|h_j}}{\tilde{u}_{|h_i}}\right)^3 = \frac{\eta_i}{\eta_j}\left(\frac{-h_i+p\eta_i}{-h_j+p\eta_j}\right)^2, \quad (i,j) = (1,2),(3,4),$$

where

$$\eta_i = 1+\frac{h_i}{E}, \quad i = 1,2,3,4.$$

We can solve this equation to arrive at an explicit expression of $p$:

$$p = \frac{h_1-\rho_{12}h_2}{\eta_1-\rho_{12}\eta_2} = \frac{h_3-\rho_{34}h_4}{\eta_3-\rho_{34}\eta_4}, \tag{33}$$

where

$$\rho_{ij} = \pm\sqrt{\frac{\eta_j}{\eta_i}\left(\frac{\tilde{u}_{|h_j}}{\tilde{u}_{|h_i}}\right)^3}, \quad (i,j) = (1,2),(3,4).$$

The value of $E$ is to be determined from eqn (33) by some iterative numerical method. Equation (33) can have more than one root (solution). It is suggested that we may observe the physical plausibility of $E$, which is equal to the tangent of the main path, to select the appropriate one, and then the value of $p$ is to be determined uniquely by eqn (33).

With the use of a few sets of four different values of $h_i$ $(i = 1,2,3,4)$, we can arrive at as many different estimates of $E$, say $(E_i \mid i = 1,2,\ldots)$. Then the location $(u_c^0,f_c^0)$ can be determined as a point where the variance among $(E_i \mid i = 1,2,\ldots)$ is minimized. Then eqns (27) and (24), respectively, yield the following pair of expressions of $q\varepsilon$:

$$\begin{aligned} q\varepsilon &= \pm\left[\operatorname{sign}(s)\left(1+\frac{h}{E}\right)\left[-h+p\left(1+\frac{h}{E}\right)\right]^2(\tilde{u}_{|h})^3\right]^{1/2} \\ &= \pm\left[-\frac{4}{27}\operatorname{sign}(s)\frac{1}{p}(\tilde{f}_c)^3\right]^{1/2}. \end{aligned} \tag{34}$$

The values of all the parameters in the asymptotic force vs displacement curve (21), accordingly, can be obtained in a systematic manner. It is to be emphasized that the present procedure with eqn (34) is quite robust and applicable in the case where the peak of an experimental case is missing and hence $\tilde{f}_c$ cannot be observed; such is often the case with the materials subject to a sudden rupture or a failure by cracking.

### 3.2. Recovery from a series of imperfect paths

When multiple experimental curves undergoing bifurcation with presumably the same bifurcation point but with different values of initial imperfections are considered, we may use the following method proposed by Ikeda et al. (1997b) that is quite robust against experimental errors to determine the location of the bifurcation point and the values of the parameters.

First, the symmetry of the displacement under consideration is to be investigated. Next the location of the bifurcation point may be determined using a single value of $h$ by repeating the following:

(1) Assume the location $(u_c^0, f_c^0)$ of the bifurcation point, shown as ($\bigcirc$) in Fig. 3(b), and obtain the incremental displacements $\tilde{u}_{|h}$ at the intersection points, shown as ($\triangle$), of the straight line $\tilde{f} + h\tilde{u} = 0$ with the experimental $f$ vs $u$ curves. Then plot $\tilde{f}_c$ against $\tilde{u}_{|h}$ for all curves.
(2) Modify the location $(u_c^0, f_c^0)$ so that the fitting (measured, e.g., in terms of the correlation coefficient) of relationship (28) is improved.

Finally, the values of the parameters are determined as follows:

(1) Choose the value of $E$, which is equal to the tangent of the main path for the perfect system, in such a manner that the main path given by eqn (25) relates experimental curves in the region sufficiently away from the bifurcation point.
(2) The value of $p$, which is associated with the tangent of the bifurcation path, can be determined by substituting the value of $E$ into the formula (29) for $\gamma^*$, the value of which is given by the tangent of the $\tilde{u}_{|h}$ vs $\tilde{f}_c$ relationship.
(3) The value of $q\varepsilon$ for each imperfect curve is evaluated by means of the Koiter law (6) with the use of the maximum load $f_c$ of the curve.

### 3.3. Use of stochastic theory of imperfection sensitivity

The multiplicity of a bifurcation point cannot be known only from the asymptotic laws for a symmetric displacement since these laws hold both for simple and double points of bifurcation. In addition, although the observation in the symmetry of the bifurcating branch may be a useful alternative to identify the type of bifurcation point (cf Ikeda et al., 1997b), such observation is often difficult during experiments. To determine the multiplicity we can make use of the stochastic variation of the critical load $f_c$ among specimens, which varies with the multiplicity of a bifurcation point (cf Murota and Ikeda, 1992; Ikeda and Murota, 1993).

Let us assume that the imperfection pattern vector $\mathbf{d}$ in eqn (3) is subject to a multivariate normal distribution with a mean $\mathbf{0}$. The probability density functions $\phi$ of the critical load $f_c$ for a simple, unstable, symmetric bifurcation point and a double, unstable one, respectively, read:

$$\phi_{fc}(f_c) = \begin{cases} \dfrac{3|f_c - f_c^0|^{1/2}}{\sqrt{2\pi}C^{3/2}} \exp\left(\dfrac{-1}{2}\left|\dfrac{f_c - f_c^0}{C}\right|^3\right), \quad -\infty \leqslant f_c \leqslant f_c^0 \\ \text{at simple, unstable, symmetric bifurcation point,} \\ \dfrac{3(f_c - f_c^0)^2}{2C^3} \exp\left(\dfrac{-|f_c - f_c^0|^3}{2C^3}\right), \quad -\infty \leqslant f_c \leqslant f_c^0 \\ \text{at double, unstable bifurcation point with } \hat{n} \geqslant 5, \end{cases} \tag{35}$$

where $C$ is a constant associated with the variance. The mean $\mathrm{E}[f_c]$ and the variance $\mathrm{Var}[f_c]$ of $f_c$ are expressed, respectively, as

$$\begin{cases} \mathrm{E}[f_c] = f_c^0 - 0.802C, \quad \mathrm{Var}[f_c] = (0.432C)^2 \\ \text{at simple, unstable, symmetric bifurcation point,} \\ \mathrm{E}[f_c] = f_c^0 - 1.13C, \quad \mathrm{Var}[f_c] = (0.409C)^2 \\ \text{at double, unstable bifurcation point with } \hat{n} \geqslant 5. \end{cases} \tag{36}$$

By equating the sample mean and variance with $\mathrm{E}[f_c]$ and $\mathrm{Var}[f_c]$ in the expressions above, we can estimate the value of $f_c^0$. We may then compare this with the value obtained based on the procedure presented in Section 3.1 or Section 3.2 to determine the multiplicity of the bifurcation point.

## 4. Numerical examples

The validity of the asymptotic formulas presented in Section 2 is confirmed based on the computational results on structural models.

### 4.1. Rectangular plates

We consider here as examples of simple, stable, symmetric bifurcation points, the elastic bifurcation analysis of a pair of four-sides-simply-supported rectangular plates subject to in-plane pure bending to in-plane pure compression. The details of this analysis can be found in Nakazawa et al. (1996). The depth-thickness ratio is chosen to be $\beta \equiv b/t = 200$, and the aspect ratio to be $\alpha \equiv a/b = 0.8$ for the pure bending and 1.0 for the pure compression, respectively, where $t$, $a$ and $b$ denote the thickness, the width and the depth of the plate, respectively.

This plate undergoes a bifurcation process with a symmetry reduction: $\mathrm{D}_1 \to \mathrm{C}_1$ in association with the loss of up-side-down symmetry. The initial imperfection is imposed in terms of an initial deflection of

$$\varepsilon \sin\left(\frac{\pi x}{a}\right) \sin\left(\frac{\pi y}{b}\right), \quad 0 \leqslant x \leqslant a, \quad 0 \leqslant y \leqslant b,$$

which is of the same pattern as the bifurcation mode. The out-of-plane deflection $u$ normalized with respect to the thickness $t$ of the plate is measured from the center line of the plate at

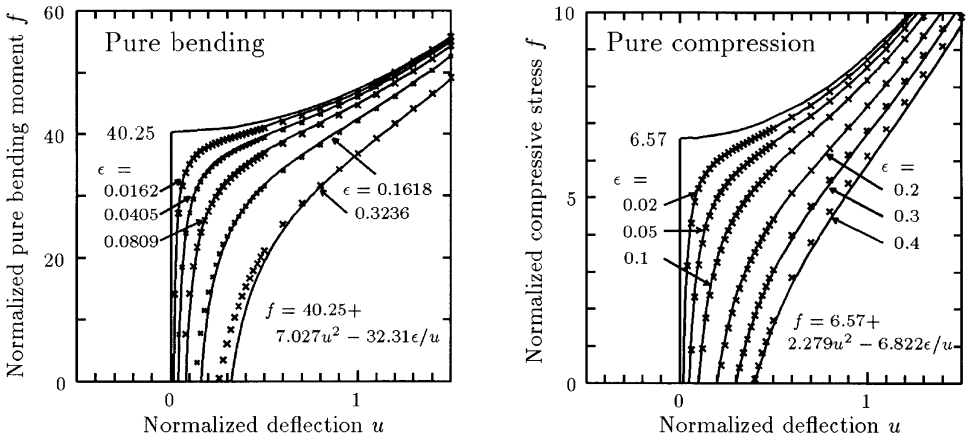


Fig. 4. Equilibrium paths of the plate. (—) denotes an equilibrium path and (×) indicates the simulation.

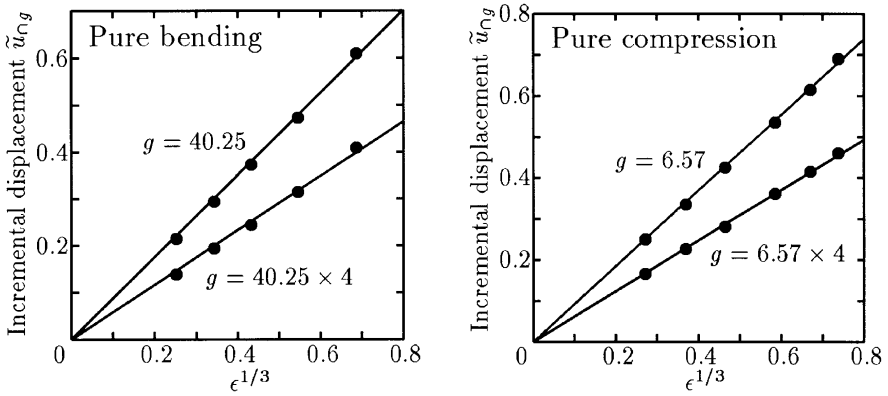


Fig. 5. $\tilde{u}_{\cap g}$ vs $\varepsilon^{1/3}$ relationship of the plate.

$(x, y) = (0.5a, 0.7b)$ for the pure bending and at $(x, y) = (0.5a, 0.5b)$ for the pure compression, respectively. This falls in the category of the nonsymmetric displacement treated in Section 2.3.1.

The solid lines in Fig. 4 shows a series of equilibrium paths computed for various values of $\varepsilon$. Then, we obtain the value of $u_{\cap g}$ of the intersection point of the parabola (8) with the imperfect $f$ vs $u$ curves ($\varepsilon \neq 0$). The $\tilde{u}_{\cap g}$ vs $\varepsilon^{1/3}$ relationship for the plate in Fig. 5 displays accurate linearity associated with the asymptotic law (9).

The computational curves are accurately simulated by a series of points shown by (×) in Fig. 4 that are computed from the bifurcation eqn (16). Unlike in experimental curves, the location of the bifurcation point and the bifurcation curve are known in this analysis. The values of the parameters in eqn (16), accordingly, were chosen as follows (without resort to the procedure presented in Section 3.2):

(1) $E$ is set to $\infty$, since the main path of the prefect system is given by $u = 0$.

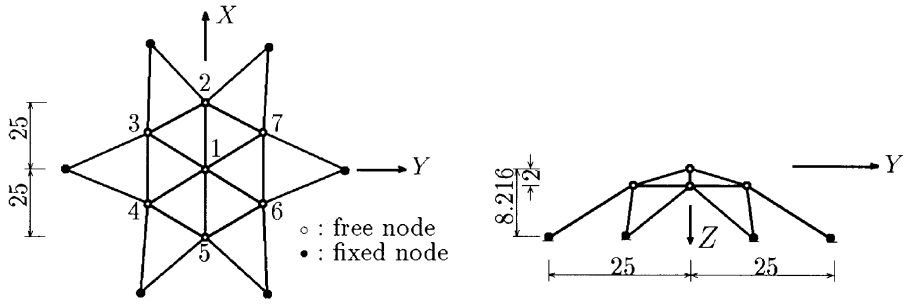


Fig. 6. Regular hexagonal ($D_6$-invariant) truss dome (unit in cm).

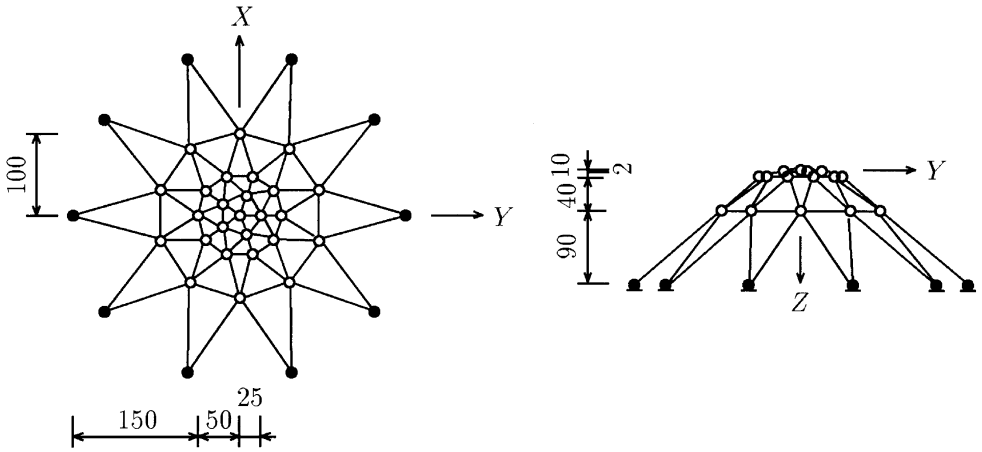


Fig. 7. Regular pentagonal ($D_5$-invariant) truss dome (unit in cm).

(2) $p^*$ is determined so that $\tilde{f}+p^*\tilde{u}^2 = 0$ approximates well the bifurcation path.
(3) $q^*$ is determined so that the slope of the $\tilde{u}_{\cap g}$ vs $\varepsilon^{1/3}$ relationship in Fig. 5 is equal to the slope $[q^*/(g-p^*)]^{1/3}$ of the law (18).

### 4.2. Regular polygonal truss domes

A regular-hexagonal ($D_6$-invariant) truss dome[1] in Fig. 6 serves as a numerical example of a simple, unstable, symmetric point of bifurcation, whereas the regular pentagonal ($D_5$-invariant) one in Fig. 7 as a group-theoretic double point with an index $\hat{n} \geqslant 5$. All members of these domes have the same modulus of elasticity and the same cross section. A vertical ($Z$-directional) load $0.5f$ is applied to the crown node 1 and a uniform vertical load $f$ to each of other free nodes.

[1] The perfect bifurcation of this dome was analyzed also by Healey (1988) in the framework of the group-theoretic bifurcation theory with an emphasis on the exploitation of symmetry.

*4.2.1. Simple bifurcation point*

For the $D_6$-invariant regular-hexagonal dome in Fig. 6, as initial imperfections, the initial location of the nodes 3, 5 and 7 are lifted upwards in the $Z$-direction at a length of $\varepsilon$, respectively. The nonlinear equilibrium eqn (1) of the dome is solved for the values of the initial imperfection $\varepsilon$ of 0, 0.01, 0.03, 0.1 and 0.3 to obtain the main and the bifurcation path shown by the dashed line and the imperfect paths shown by the solid lines in Fig. 8. The symbol (○) in this figure denotes a simple, unstable, symmetric bifurcation point. The $Z$-directional components of the critical eigenvector, which represent a bifurcation mode, at this point are schematically depicted in Fig. 9. This mode has the rotation symmetry with respect to a rotation around $Z$-axis at an angle of $2\pi/3$ and the reflection symmetry with respect to the three vertical planes that, respectively, pass the lines 2-1-5, 3-1-6 and 4-1-7, and therefore is $D_3$-invariant. Thus the bifurcation point is related to a symmetry-breaking process : $D_6 \rightarrow D_3$, and hence is associated with the one-dimensional irreducible representation $(\delta, j) = (1, 3)$ in eqn (A16). The $Z$-coordinate of the first node $z_1$ in Fig. 6, which is used as the abscissa in Fig. 8(a), is $D_6$-invariant, and hence corresponds to the case of a symmetric ($D_6$-invariant) displacement with $\eta_{i*1} = 0$ in Section 2.3. In contrast, the second node $z_2$ in (b) in

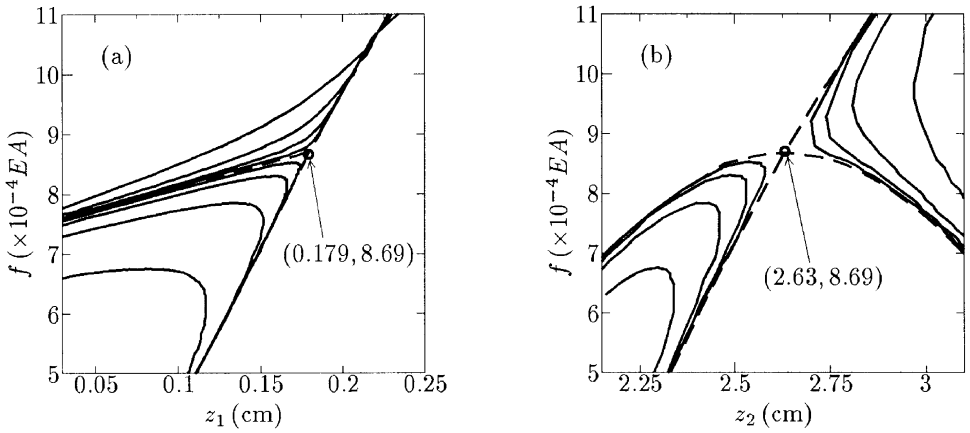


Fig. 8. Equilibrium paths of the hexagonal truss dome. (a) $f$ vs $z_1$ curve. (b) $f$ vs $z_2$ curve. (—) denotes a curve for an imperfect system, (- - -) indicates that for a perfect one, and (○) represents a bifurcation point.

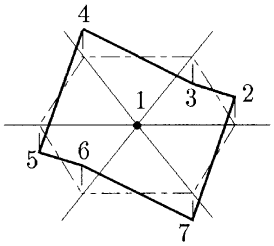


Fig. 9. Bird's-eye view of the $Z$-directional components of the bifurcation mode at the bifurcation point of the hexagonal dome.

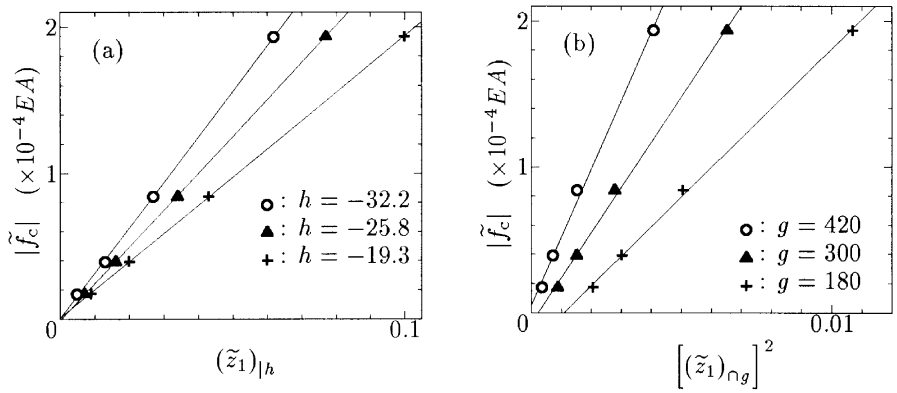


Fig. 10. The application of the asymptotic laws to a $D_6$-invariant displacement $z_1$. (a) $\tilde{f}_c$ vs $(\tilde{z}_1)_{|h}$ relationship. (b) $\tilde{f}_c$ vs $[(\tilde{z}_1)_{\cap g}]^2$ relationship.

Fig. 6, which is used as the abscissa in Fig. 8(b), is not $D_6$-invariant and corresponds to the case of a non $D_6$-invariant displacement with $\eta_{i^*1} \neq 0$ in Section 2.3.

First the applicability of the asymptotic laws to the $D_6$-invariant displacement $z_1$ is investigated. Whereas the law (28) is expected in this case, another law (19) for a non-$D_6$-invariant displacement is used for comparison. The intersection points of the imperfect paths and the straight line $\tilde{f}+h\tilde{z}_1 = 0$ of eqn (26) and those of the paths and the parabola $\tilde{f}+g\tilde{z}_2^2 = 0$ of eqn (17) are obtained for various values of $h$ and $g$. Figure 10 shows $|\tilde{f}_c|$ vs $(\tilde{z}_1)_{|h}$ relationship in (a) and $|\tilde{f}_c|$ vs $[(\tilde{z}_1)_{\cap g}]^2$ one in (b). The straight lines, which denote the least square approximation to the data, pass the close neighborhood of the origin in (a) and not in (b). Thus, the present computational results are in good agreement with the asymptotic law in eqn (28), which represents a straight line passing the origin, and fail to satisfy the other asymptotic law in eqn (19), which is not applicable to this type of displacement. The consideration of the type of displacement, accordingly, is vital in the successful application of the asymptotic laws.

Next, for the non-$D_6$-invariant displacement $z_2$, $|\tilde{f}_c|$ vs $[(\tilde{z}_2)_{\cap g}]^2$ relationship in Fig. 11 is obtained. The straight lines representing the least square approximation to the plotted data correlate well with these data and pass the origin. This assesses the validity and applicability of the law (19) that corresponds to the straight line passing the origin.

Finally, in Fig. 12(a) and (b), the equilibrium paths of the dome, shown by the solid lines in (a) and (b), are simulated by the asymptotic curves, shown by the dashed lines, which are computed by eqns (21) and (16), respectively. The asymptotic curves are very close to the equilibrium paths for (a) and fairly close for (b). We could determine the values of the parameters $E$, $p$, $q\varepsilon$, $p^*$ and $q^*\varepsilon$ in these equations using the procedure described in Section 3.1, but we here adopt the following alternative procedure to show another possibility:

- The value of $E$ was chosen in such a manner that the asymptotic curve is tangential to the computational one at the bifurcation point.
- For $D_6$-invariant displacement, the value of $p$ was chosen in view of the relationship that the value of the slope of the straight line in Fig. 10(a) is equal to $\gamma^*$ in (29). The value of $q\varepsilon$ was chosen based on the Koiter law (24).

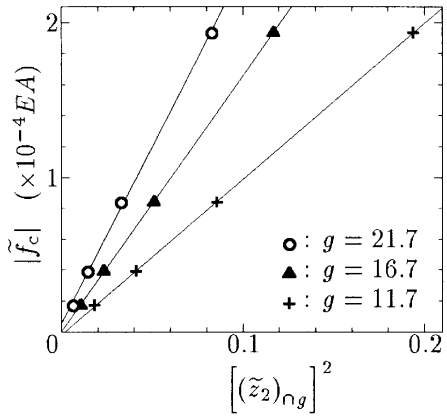


Fig. 11. The application of the asymptotic law (28) to a non-$D_6$-invariant displacement $z_2$ ($\tilde{f}_c$ vs $[(\tilde{z}_2)_{\cap g}]^2$ relationship).

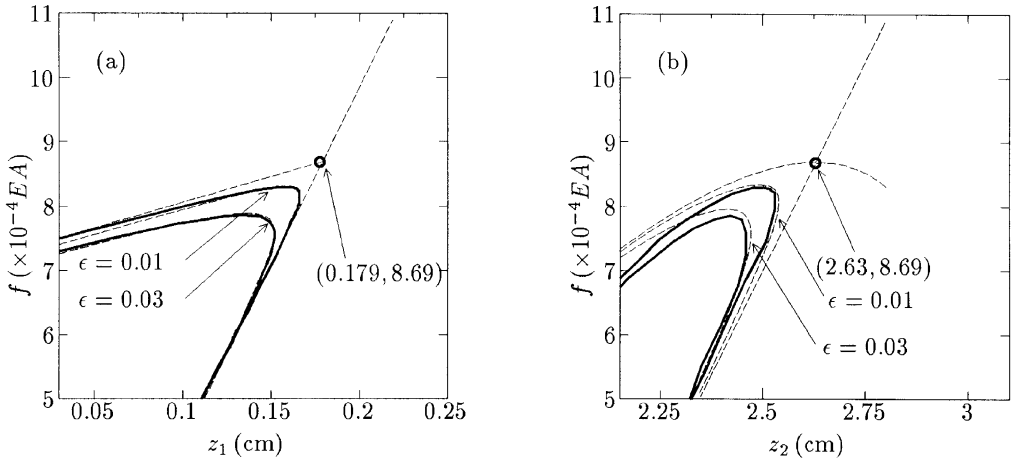


Fig. 12. The simulation of the equilibrium paths of the hexagonal truss dome by the asymptotic curves. (a) $f$ vs $z_1$ curve. (b) $f$ vs $z_2$ curve. (—) denotes a computational curve, (- - -) indicates an asymptotic one, and (○) represents a bifurcation point.

- For non-$D_6$-invariant displacement, the value of $p^*$ was chosen such that the value of the slope of the straight line in Fig. 11 is equal to the tangent of the relationship (19), and the value of $q^*\varepsilon$ by the Koiter law (6).

*4.2.2. Double bifurcation point*

The $D_5$-invariant regular-pentagonal dome in Fig. 7 is considered as an example of a system with a double bifurcation point with an index $\hat{n} \geqslant 5$. As initial imperfections, the initial location of the nodes 2–6 are displaced in the $Z$-direction. The amount of the initial displacement of each node was given randomly to simulate (physical) experiments, in which the pattern and the mag-

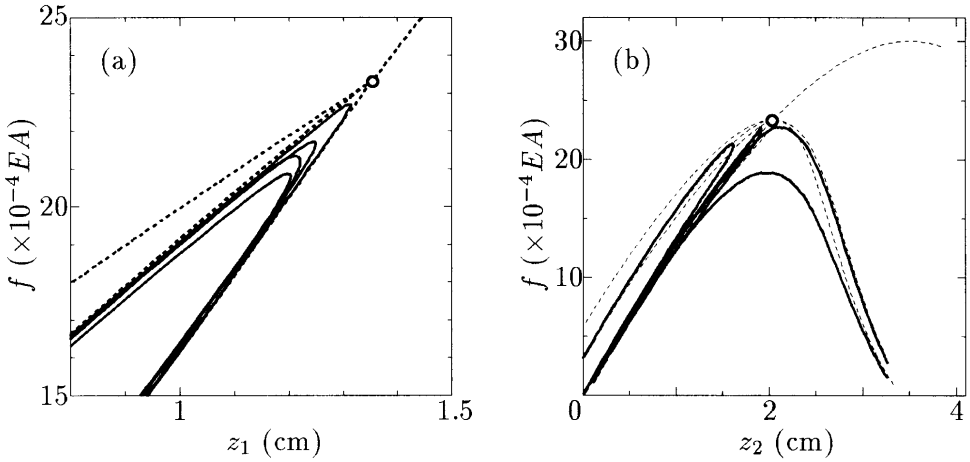


Fig. 13. Equilibrium paths of the pentagonal truss dome obtained through computation. (a) $f$ vs $z_1$ curves. (b) $f$ vs $z_2$ curves. (—) denotes an imperfect curve, (- - -) indicates a perfect one, and (○) is a bifurcation point.

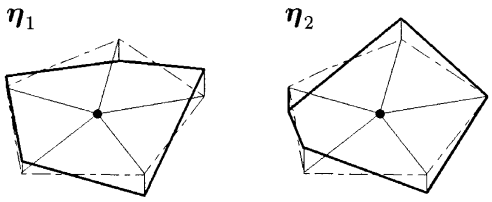


Fig. 14. Bird's-eye view of the $Z$-directional components of the inner pentagonal nodes for a pair of bifurcation modes at the double bifurcation point of the pentagonal dome.

nitude of the initial imperfections cannot be known *a priori*. The solid lines in Fig. 13(a) and (b) show some instances of equilibrium paths computed for those initial imperfections. The vertical displacement $z_1$ for the center node used as the abscissa in (1) is $D_5$-invariant, whereas $z_2$ for an outer node is not. The dashed lines in this figure denote the paths for the perfect system ($\varepsilon = 0$), and the symbol (○) denotes a double, unstable bifurcation point with an index $\hat{n} = 5$. The $Z$-directional components of the inner pentagonal nodes of the pair of critical eigenvectors $\boldsymbol{\eta}_1$ and $\boldsymbol{\eta}_2$ at this point are depicted in Fig. 14. The mode for $\boldsymbol{\eta}_1$, which has the reflection symmetry with respect to a vertical plane, is $D_1$-invariant, whereas that for $\boldsymbol{\eta}_2$ lacking the reflection symmetry is $C_1$-invariant. This bifurcation point is related to a symmetry-breaking process:[2] $D_5 \to D_1^j$ ($j = 1, \ldots, 5$) with an index of $\hat{n} = 5$. It is well known that $2\hat{n} = 10$ half branches exist at this double bifurcation point (cf e.g., Ikeda et al., 1991).

First, we consider the $D_5$-invariant vertical displacement $z_1$ of the node 1, for which the asymp-

[2] This bifurcation point is associated with the two-dimensional irreducible representation $(\delta, j) = (2, 2)$ defined by eqn (A15).

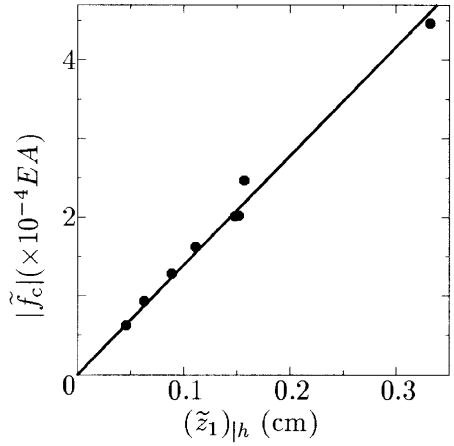


Fig. 15. The application of the asymptotic law (28) for a $D_5$-invariant displacement to the pentagonal truss dome [$|\tilde{f}_c|$ vs $(\tilde{z}_1)_{|h}$ relationship for $h = -0.1388$].

totic laws (21)–(29) are applicable. The $|\tilde{f}_c|$ vs $(\tilde{z}_1)_{|h}$ relationship plotted in Fig. 15 correlates well with the asymptotic law in (28) that represents a straight line passing the origin (the correlation coefficient is 0.994).

Next, let us consider the vertical displacement $z_2$ of the node 2, which is not $D_5$-invariant. Unlike for simple bifurcation points, no asymptotic laws are applicable to this non-$D_5$-invariant displacement. There are as many as six $f$ vs $z_2$ curves bifurcating from the point, as shown in Fig. 13(b). Owing to the presence of so many bifurcating curves, the simulation is not possible.

A set of 50 imperfect equilibrium paths are obtained by imposing normally-distributed initial imperfections on the $Z$-directional components of the free nodes of the pentagonal dome. The stochastic theory of initial imperfections presented in Section 3.3 is applied to this case. The histogram of the maximum loads $f_c$ is compared with the probability density functions (35) for a simple, unstable, symmetric point and a double bifurcation point in Fig. 16, where the abscissa indicates a normalized critical load $\zeta = (f_c - f_c^0)/C$. The use of the sample values

$$\mathrm{E}[f_c] = 22.16 \times 10^{-4} EA, \quad \mathrm{Var}[f_c] = 0.1262 \times (10^{-4} EA)^2$$

of $f_c$ in eqn (36) results in the values of $f_c^0$ and $C$,

$$\begin{cases} f_c^0 = 22.82 \times 10^{-4} EA, \quad C = 0.8214 \times 10^{-4} EA, \\ \text{assuming simple, symmetric bifurcation point,} \\ f_c^0 = 23.14 \times 10^{-4} EA, \quad C = 0.8686 \times 10^{-4} EA, \\ \text{assuming double bifurcation point.} \end{cases} \tag{37}$$

The substitution of these values of $f_c^0$ and $C$ into eqn (35) gives the probability density function of $f_c$ shown in Fig. 16. The statistical estimate $f_c^0 = 23.14 \times 10^{-4} EA$ for the double point in eqn (37) is much closer to the exact value $f_c^0 = 23.32 \times 10^{-4} EA$, in comparison with $f_c^0 = 22.82 \times 10^{-4} EA$ estimated for the simple, symmetric bifurcation point. Hence we conclude that the bifurcation

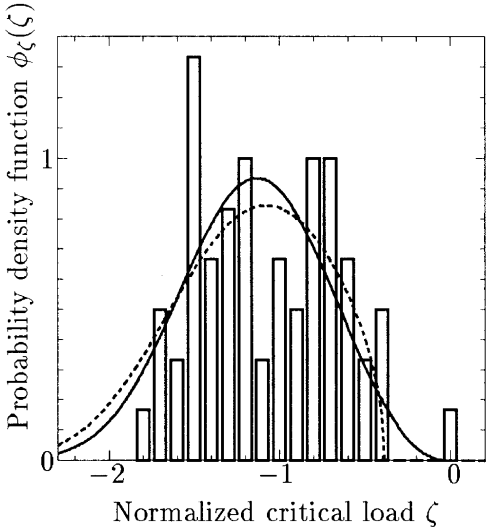


Fig. 16. Histogram and the curves of probability density function of the normalized critical load $\zeta = (f_c - f_c^0)/C$ for 50 imperfect regular-pentagonal domes. (- - -) indicates a curve for a simple, unstable, symmetric bifurcation point and solid one (—) that for a double, unstable bifurcation point.

point is a double point. The observation of the stochastic scatter of critical loads, in this manner, enables us to determine the multiplicity of a bifurcation point if the value of $f_c^0$ (or its estimate somehow obtained) is available.

## 5. Experimental examples

We investigate the applicability of the asymptotic laws presented in Section 2 and of the procedure for recovering the curve for the perfect system presented in Section 3 to cylindrical sand specimens subject to triaxial compression test.

### 5.1. Procedure for a single curve

As an example of a single curve, we refer to the experimental data of Ikeda et al. (1997b) for the triaxial compression test on Toyoura sand specimens with a diameter of 7 cm and a height of 10 cm. The initial void ratio was aimed at 0.66. These specimens with lubricated ends under drained condition were subject to a confining pressure $\sigma_3$ of 98 kPa (1.0 kgf/cm$^2$).

The technique of the search of the bifurcation point is applied to a pair of specimens 4-4 and 8-1. Figure 17 shows the $\sigma$ vs $\varepsilon_a$ curves of these specimens and the rectangular areas employed for the search, whereas Fig. 18 shows the distribution of the inverse $1/\mathrm{Var}[E]$ of the variance $\mathrm{Var}[E]$ among $E_i$ $(i = 1, 2, \ldots)$ in the rectangular areas of $(\varepsilon_a, \sigma)$ in Fig. 17. Here $\sigma = \sigma_1 - \sigma_3$ indicates the deviator stress ($\sigma_1$ is the axial stress). This figure clearly shows for each specimen the presence of the location of local minimum, which corresponds to the bifurcation point. In the course of the search, the values of the parameters $p$, $E$, and $q\varepsilon$ have been obtained for each specimen.

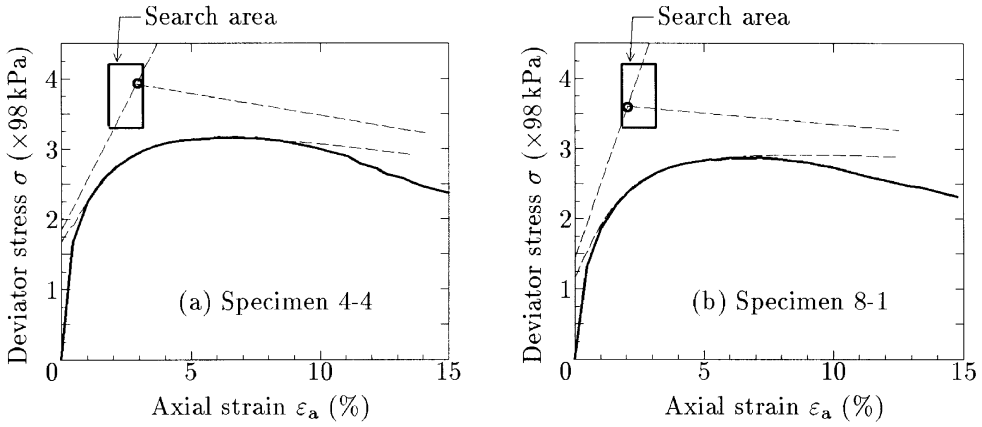


Fig. 17. Simulation of a pair of curves of deviator stress vs axial strain ($\sigma$–$\varepsilon_a$) for sand specimens. (a) Specimen 4-4 [$(\varepsilon_a)_c^0 = 2.89$, $\sigma_c^0 = 3.92$, $p = 0.0573$, $E = 0.717$ and $q\varepsilon = 1.092$]. (b) Specimen 8-1 [$(\varepsilon_a)_c^0 = 2.04$, $\sigma_c^0 = 3.60$, $p = 0.0311$, $E = 1.057$ and $q\varepsilon = 1.250$]. (—) denotes an experimental (imperfect) curve, (- - -) indicates a computed one, and (○) represents a bifurcation point.

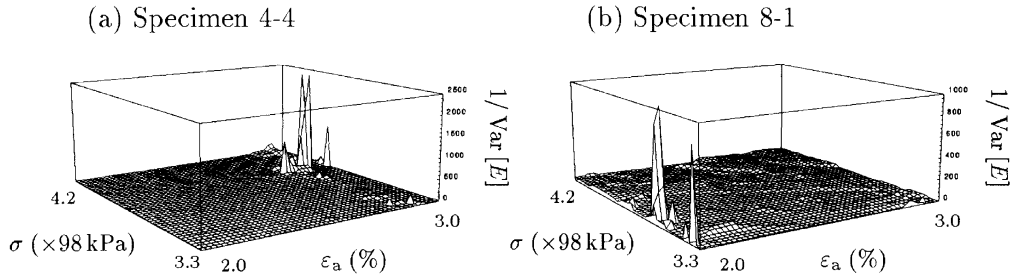


Fig. 18. The distribution of the inverse of the variance Var[$E$] among $E_i$ ($i = 1, 2, \ldots$) in the rectangular areas of ($\varepsilon_a$, $\sigma$) in Fig. 17.

Figure 17 shows the simulation of the curves of deviator stress vs axial strain ($\sigma$–$\varepsilon_a$) for the two specimens by eqn (21), with the use of the values of the parameters obtained by the search. The theoretical curves correlate fairly well with the experimental ones, especially in the vicinity of the bifurcation point. This is in agreement with the local nature of the present theory that is more accurate in the vicinity and less accurate away from the point; such inaccuracy away from it may be attributed also to plasticity. Note that the simulation carried out here is not the curve fitting by artificial choice of the values of parameters since the values of all parameters were uniquely determined based on the search strategy.

### 5.2. *Procedure for a series of curves*

As an example of a series of curves, we refer to a set of 32 experimental curves of stress vs strain of cylindrical sand specimens (see, Ikeda and Murota, 1996 for more details). These specimens had a constant diameter $D$ of 7 cm and a height $H$ of 15 cm. The initial void ratio $e_0$ was controlled

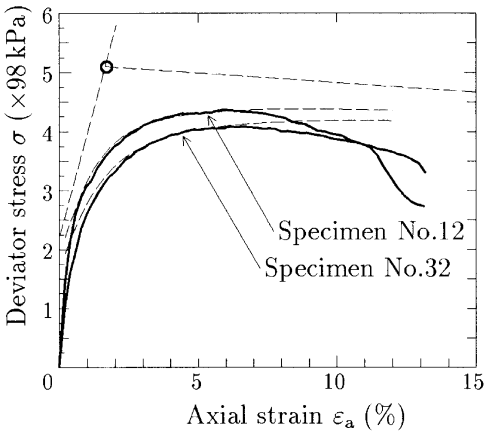


Fig. 19. Simulation of the curves of deviator stress vs axial strain ($\sigma$–$\rho_a$) for sand specimens. [$(\varepsilon_a)_c^0 = 1.65$, $\sigma_c^0 = 5.10$, $p = 0.0319$, $E = 1.75$ and $q\varepsilon = 1.31$ for No. 12 and 1.88 for No. 32]. (—) denotes an experimental (imperfect) curve, (- - -) indicates a computed one, and (○) represents a bifurcation point.

to the range of $0.67 < e_0 < 0.69$. These specimens with fixed ends under drained condition were made of fresh saturated Toyoura sand subject to a confining pressure of 98 kPa (1.0 kgf/cm$^2$). Examples of experimental curves of deviator stress $\sigma$ vs axial strain $\varepsilon_a$ are shown in Fig. 19.

The initial states for the specimens are assumed to be $D_n$-invariant with $n$ large. Among the possible bifurcation points of this system, we restrict ourselves to a simple, symmetric bifurcation point and a double bifurcation point with $\hat{n} \geqslant 5$, which are associated, respectively, with the symmetry-breaking processes:

$$\begin{cases} D_n \to C_n & \text{at simple, symmetric bifurcation point,} \\ D_n \to D_m & \text{at double bifurcation point } (\hat{n} \geqslant 5). \end{cases}$$

In order to determine the type of displacement and of the bifurcation point, we refer to the asymptotic laws and the stochastic theory of imperfection sensitivity (cf, Section 3.3). Since the observed variable, axial strain $\varepsilon_a$, is $D_n$-invariant, the asymptotic law (28) for a $D_n$-invariant displacement of a simple, symmetric bifurcation point or a double bifurcation point is expected to be applicable in the present case.

The asymptotic law (28) for a $D_n$-invariant displacement is employed. Unlike for the computational results in the previous section, the paths for the perfect system and the location of the bifurcation point cannot be known *a priori*. Therefore, a systematic search in the two-dimensional space of $(\varepsilon_a, \sigma)$ with a sufficiently fine mesh was carried out in order to choose the location where the value of the correlation coefficient of relationship (28) is maximized to be a bifurcation point $((\varepsilon_a)_c^0, \sigma_c^0)$. The $|\tilde{\sigma}_c|$ vs $(\tilde{\varepsilon}_a)_{|h}$ relationship for the 32 sets of data plotted in Fig. 20 is in good agreement with the straight line passing the origin that corresponds to the asymptotic law in eqn (28); the correlation coefficient is equal to 0.980.

Figure 19 shows the simulation of the curves of axial strain vs deviator stress ($\varepsilon_a$–$\sigma$) for the two specimens by eqn (21), with the use of the values of the parameters that were chosen based on the

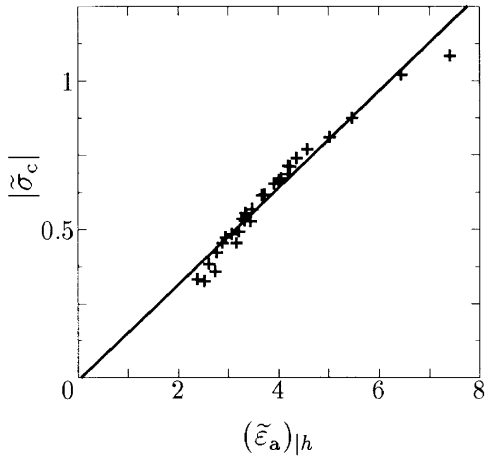


Fig. 20. The $|\tilde{\sigma}_c|$ vs $(\tilde{\varepsilon}_a)_{|h}$ relationship ($h = 0.17$) of the sand specimens $[((\varepsilon_a)_c^0, \sigma_c^0) = (1.65, 5.10)]$.

procedure presented in Section 3.2. The theoretical curves correlate fairly well with the experimental ones.

As we have seen in Fig. 20, the law (28) for a $D_n$-invariant displacement had much better correlation with the experimental data than the law (19) for a non-$D_n$-invariant one, in agreement with the aforementioned expectation. An appropriate choice of a law has thus resulted in a better correlation.

In order to determine the multiplicity of the bifurcation point, which cannot be determined merely from the asymptotic law (28), we employ the stochastic theory of imperfection sensitivity (cf, Section 3.3). The histogram of the maximum deviator stress for those specimens is compared in Fig. 21 with the probability density functions for a simple, unstable, symmetric and for a double

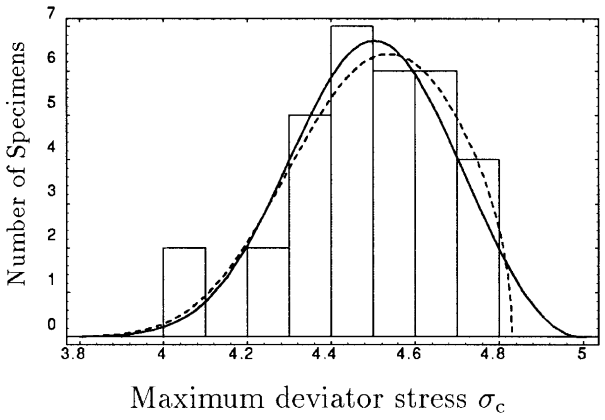


Fig. 21. Histogram and the curves of probability density function of the maximum deviator stress $\sigma_c$ for 32 sand specimens. (- - -) indicates a curve for a simple, unstable, symmetric bifurcation point and (—) that for a double, unstable bifurcation point.

bifurcation point. The values of the sample mean $E[\sigma_c]$ and the sample variance $Var[\sigma_c]$ of the maximum deviator stress, respectively, are: $E[\sigma_c] = 4.49$ and $Var[\sigma_c] = 0.0335$. The use of these values in eqn (36) results in the estimated values of $\sigma_c^0$ and $C$,

$$\begin{cases} \sigma_c^0 = 4.83(\times 98\,\text{kPa}), \quad C = 0.424(\times 98\,\text{kPa}) \\ \text{assuming simple, symmetric bifurcation point,} \\ \sigma_c^0 = 4.96(\times 98\,\text{kPa}), \quad C = 0.448(\times 98\,\text{kPa}) \\ \text{assuming double bifurcation point.} \end{cases} \tag{38}$$

The substitution of these values of $\sigma_c^0$ and $C$ into eqn (35) gives the probability density function of $\sigma_c$ shown by the solid and dashed curves in Fig. 21. The two possible values of $\sigma_c^0$ in eqn (38) are to be compared with the target value $\sigma_c^0 = 5.10$ obtained from the $|\tilde{\sigma}_c|$ vs $(\tilde{\varepsilon}_a)_{|h}$ relationship in Fig. 20(a). Evidently, the value $\sigma_c^0 = 4.96$ for the double point in eqn (38) is much closer to the target value $\sigma_c^0 = 5.10$ than $\sigma_c^0 = 4.83$ for the simple symmetric bifurcation point is. Based on this, it is concluded that the bifurcation point is more likely to be a double point.

## 6. Conclusions

A series of pertinent asymptotic laws for physically observable displacements for systems with dihedral group symmetry undergoing bifurcation have been presented in order to make the results of bifurcation theory hitherto developed applicable to bifurcation observed in experiments. As we have seen through the application to numerical and experimental examples, the whole set of laws are capable of describing various aspects of bifurcation behavior in a consistent manner. In the successful physical interpretation of experimental curves subject to bifurcation, it is vital to identify the symmetry of the observed displacement and the type of bifurcation point, because the asymptotic formulas to be employed vary depending on the symmetry and the type. This paper hopefully has offered a step towards such success, whereas the group-theoretic bifurcation theory serves as a supplementary means to identify the type of bifurcation point through the observation of the shape and deformation pattern of a specimen (Ikeda et al., 1997b).

The perfect curve of a system has been constructed based on a single or a number of experimental curves. This perfect curve offers us the insight into the mechanism of bifurcation behavior, and hence is vital in arriving at the true constitutive relationship. A dual viewpoint of bifurcation and plasticity, accordingly, will be needed in the future study of constitutive relationship.

## Acknowledgements

The authors would like to thank Dr M. Nakazawa and Mr Y. Yamakawa for their enthusiastic support in the numerical analysis. The triaxial compression tests on sand specimens were supported by the Maeda Memorial Engineering Foundation.

## Appendix : $D_n$-equivariant system

Technical details of the analysis for systems with regular-polygonal (dihedral group) symmetry are presented in this Appendix. The major development is a recapitulation of Murota and Ikeda (1991), whereas Section A.5.2 and part of Section A.4 are new.

### *A.1. Group equivariance*

We consider a system of nonlinear equilibrium equations

$$\mathbf{F}(\mathbf{u}, f, \mathbf{v}) = \mathbf{0}, \tag{A1}$$

where $\mathbf{u} \in \mathbf{R}^N$ is a displacement (or position) vector, $f \in \mathbf{R}$ a loading parameter, $\mathbf{v} \in \mathbf{R}^p$ an imperfection parameter vector. We assume that the symmetry of the imperfect system is described by the equivariance of $\mathbf{F}(\mathbf{u}, f, \mathbf{v})$ in eqn (A1) to a compact group $G$:

$$T(g)\mathbf{F}(\mathbf{u}, f, \mathbf{v}) = \mathbf{F}(T(g)\mathbf{u}, f, S(g)\mathbf{v}), \quad g \in G, \tag{A2}$$

where $T(g)$ and $S(g)$ $(g \in G)$ denote unitary matrix representations of $G$ on the space $\mathbf{R}^N$ of displacement vector $\mathbf{u}$ and on the space $\mathbf{R}^p$ of imperfection parameter $\mathbf{v}$, respectively. Let us denote by $\Sigma(\mathbf{u})$ the isotropy subgroup of $\mathbf{u}$, i.e.,

$$\Sigma(\mathbf{u}) = \Sigma(\mathbf{u}; G, T) = \{g \in G | T(g)\mathbf{u} = \mathbf{u}\}. \tag{A3}$$

Similarly we denote

$$\Sigma(\mathbf{v}) = \Sigma(\mathbf{v}; G, S) = \{g \in G | S(g)\mathbf{v} = \mathbf{v}\}.$$

Henceforth we assume $\Sigma(\mathbf{v}^0) = G$, i.e., that the imperfection vector $\mathbf{v}^0$ of the perfect system is $G$-symmetric. It then follows from eqn (A2) that the perfect system $\mathbf{F}(\mathbf{u}, f, \mathbf{v}^0)$ is equivariant to $G$:

$$T(g)\mathbf{F}(\mathbf{u}, f, \mathbf{v}^0) = \mathbf{F}(T(g)\mathbf{u}, f, \mathbf{v}^0), \quad g \in G. \tag{A4}$$

We also assume $\Sigma(\mathbf{u}_c^0) = G$, i.e., that the critical point $(\mathbf{u}_c^0, f_c^0)$ of the perfect system lies on a $G$-symmetric equilibrium path. If $\Sigma(\mathbf{u}) = G$ for $(\mathbf{u}, f)$ on the path of the perfect system, the equivariance (A4) is inherited to the Jacobian as

$$T(g)J(\mathbf{u}, f, \mathbf{v}^0) = J(\mathbf{u}, f, \mathbf{v}^0)T(g), \quad g \in G. \tag{A5}$$

The Jacobian matrix is singular at the critical point $(\mathbf{u}_c^0, f_c^0)$: let $M$ be the rank deficiency (i.e., dimension of the kernel) of $J^0 = J(\mathbf{u}_c^0, f_c^0, \mathbf{v}^0)$. By eqn (A5) the kernel is $G$-invariant. The point $(\mathbf{u}_c^0, f_c^0)$ is called simple if $M = 1$ and double if $M = 2$. The point is called group-theoretic if the kernel of $J$ is $G$-irreducible and parametric otherwise. (Here the kernel space is said to be $G$-irreducible if it contains no nontrivial proper $G$-invariant subspace; it is $G$-reducible otherwise.) In this paper we shall be interested in group-theoretic critical points, which appear generically due to group symmetry.

### A.2. Liapunov–Schmidt reduction

We now reduce the whole system (A1) of $N$ equations to $M$ ($=\dim\ker J^0$) equations according to a standard procedure known as the elimination of passive coordinates (e.g., Thompson and Hunt, 1973) or the Liapunov–Schmidt reduction (e.g., Sattinger, 1979). Let $\{\boldsymbol{\xi}_j \mid j=1,\ldots,N\}$ and $\{\boldsymbol{\eta}_j \mid j=1,\ldots,N\}$ be orthonormal bases of $\mathbf{R}^N$ such that

$$\boldsymbol{\xi}_i^{\mathrm{T}} J^0 = \mathbf{0}^{\mathrm{T}}, \quad J^0\boldsymbol{\eta}_j = \mathbf{0}, \quad i,j=1,\ldots,M,$$

where $(\cdot)^{\mathrm{T}}$ denotes the transpose of a matrix. Note that $\{\boldsymbol{\xi}_i \mid i=1,\ldots,M\}$ and $\{\boldsymbol{\eta}_j \mid j=1,\ldots,M\}$ span the kernels of $(J^0)^{\mathrm{T}}$ and $J^0$, respectively. We express the displacement $\mathbf{u}$ in terms of $\mathbf{w}=(w_i \mid i=1,\ldots,N)\in\mathbf{R}^N$ as

$$\mathbf{u} = \mathbf{u}_{\mathrm{c}}^0 + \sum_{j=1}^{N} w_j\boldsymbol{\eta}_j. \tag{A6}$$

With the use of $\tilde{f}$ in eqn (2) and $\mathbf{w}$ in eqn (A6), the original system (A1) is decomposed into two parts: one system of equations for the kernel space

$$\boldsymbol{\xi}_i^{\mathrm{T}}\mathbf{F}\left(\mathbf{u}_{\mathrm{c}}^0 + \sum_{j=1}^{N} w_j\boldsymbol{\eta}_j, f_{\mathrm{c}}^0 + \tilde{f}, \mathbf{v}\right) = 0, \quad i=1,\ldots,M, \tag{A7}$$

and the other for the rank space

$$\boldsymbol{\xi}_i^{\mathrm{T}}\mathbf{F}\left(\mathbf{u}_{\mathrm{c}}^0 + \sum_{i=1}^{N} w_j\boldsymbol{\eta}_j, f_{\mathrm{c}}^0 + \tilde{f}, \mathbf{v}\right) = 0, \quad i=M+1,\ldots,N. \tag{A8}$$

By the implicit function theorem, the latter system of equations can be solved locally in the neighborhood of $(\mathbf{u}_{\mathrm{c}}^0, f_{\mathrm{c}}^0, \mathbf{v}^0)$ for $w_j$ ($j=M+1,\ldots,N$) as

$$w_j = \varphi_j(\tilde{\mathbf{w}}, \tilde{f}, \mathbf{v}), \quad j=M+1,\ldots,N,$$

where $\tilde{\mathbf{w}}=(w_i \mid i=1,\ldots,M)\in\mathbf{R}^{\mathrm{M}}$. On substituting this into eqn (A7) we obtain a reduced system of $M$ equations

$$\tilde{\mathbf{F}}(\tilde{\mathbf{w}}, \tilde{f}, \mathbf{v}) = \mathbf{0} \tag{A9}$$

in $\tilde{\mathbf{w}}\in\mathbf{R}^M$, where $\tilde{\mathbf{F}}=(\tilde{F}_i \mid i=1,\ldots,M)$ and

$$\tilde{F}_i(\tilde{\mathbf{w}}, \tilde{f}, \mathbf{v}) = \boldsymbol{\xi}_i^{\mathrm{T}}\mathbf{F}\left(\mathbf{u}_{\mathrm{c}}^0 + \sum_{j=1}^{M} w_j\boldsymbol{\eta}_j + \sum_{j=M+1}^{N} \varphi_j(\tilde{\mathbf{w}}, \tilde{f}, \mathbf{v})\boldsymbol{\eta}_j, f_{\mathrm{c}}^0 + \tilde{f}, \mathbf{v}\right)$$

($i=1,\ldots,M$). This reduced eqn (A9) is called the bifurcation equation (often with $\mathbf{v}=\mathbf{v}^0$). Referring to $\mathbf{v}=\mathbf{v}^0+\varepsilon\mathbf{d}$ in eqn (3), we fix the imperfection mode $\mathbf{d}$ and often regard $\varepsilon$ as an independent variable for imperfection $\mathbf{v}$; namely, we put

$$\hat{\mathbf{F}}(\tilde{\mathbf{w}}, \tilde{f}, \varepsilon) = \tilde{\mathbf{F}}(\tilde{\mathbf{w}}, \tilde{f}, \mathbf{v}^0 + \varepsilon\mathbf{d}). \tag{A10}$$

This is for the convenience of asymptotic analysis with sufficiently small $\varepsilon$.

The critical point $(\mathbf{u}_c, f_c)$ of an imperfect system is determined from the bifurcation eqn (A9) as its critical point, at which the Jacobian of eqn (A9) vanishes:

$$\det \tilde{J}(\tilde{\mathbf{w}}, \tilde{f}, \mathbf{v}) = 0, \tag{A11}$$

where $\tilde{J} = (\partial \tilde{F}_i / \partial w_j \mid i,j = 1, \ldots, M)$.

The bifurcation equation (A9) inherits the group equivariance of the original system (A1), that is,

$$\tilde{T}(g)\tilde{\mathbf{F}}(\tilde{\mathbf{w}}, \tilde{f}, \mathbf{v}) = \tilde{\mathbf{F}}(\tilde{T}(g)\tilde{\mathbf{w}}, \tilde{f}, S(g)\mathbf{v}), \quad g \in G, \tag{A12}$$

is satisfied for appropriate choices of $\{\boldsymbol{\xi}_i\}$ and $\{\boldsymbol{\eta}_i\}$. In this equation $\tilde{T}$ is the subrepresentation of $T$ on the $M$-dimensional kernel of $J^0 = J(\mathbf{u}_c^0, f_c^0, \mathbf{v}^0)$. Here $\tilde{T}$ is unitary since $T(g)$ is assumed to be unitary and $\{\boldsymbol{\xi}_i\}$ and $\{\boldsymbol{\eta}_i\}$ are orthonormal.

### *A.3. Regular polygonal symmetry*

We choose $G$ to be the dihedral group $\mathrm{D}_n$ of degree $n$ introduced in Section 2.4. Let

$$R(\mathrm{D}_n) = \begin{cases} \{(1,j) \mid j = 1,2,3,4\} \bigcup \{(2,j) \mid j = 1, \ldots, (n-2)/2\} & \text{for } n \text{ even}, \\ \{(1,j) \mid j = 1,2\} \bigcup \{(2,j) \mid j = 1, \ldots, (n-1)/2\} & \text{for } n \text{ odd}, \end{cases} \tag{A13}$$

be the index set of all nonequivalent real irreducible representations of $\mathrm{D}_n$, where the first component $\delta$ of the index $(\delta, j)$ indicates the dimension.

The one-dimensional irreducible representations $(1,j)$ are defined by

$$T^{(1,j)}(c(2\pi/n)) = \begin{cases} 1 & \text{if } j = 1,2, \\ -1 & \text{if } j = 3,4; \end{cases} \quad T^{(1,j)}(\sigma) = \begin{cases} 1 & \text{if } j = 1,3, \\ -1 & \text{if } j = 2,4. \end{cases} \tag{A14}$$

The two-dimensional representations $(2,j)$ can be chosen such that

$$T^{(2,j)}(c(2\pi/n)) = \begin{pmatrix} \cos(2\pi j/n) & -\sin(2\pi j/n) \\ \sin(2\pi j/n) & \cos(2\pi j/n) \end{pmatrix}, \quad T^{(2,j)}(\sigma) = \begin{pmatrix} 1 & 0 \\ 0 & -1 \end{pmatrix}. \tag{A15}$$

Since the kernel of $J^0$ is $\mathrm{D}_n$-invariant, as noted before, it is generically a $\mathrm{D}_n$-irreducible subspace. Hence, generically, the critical point $(\mathbf{u}_c^0, f_c^0)$ is either simple or double, according to whether it is associated with a one-dimensional irreducible representation $(1,j)$ (for some $j$) or a two-dimensional one $(2,j)$ (for some $j$).

For a simple critical point, we note that

$$\Sigma(\boldsymbol{\xi}_1) = \Sigma(\boldsymbol{\eta}_1) = \mathrm{D}_n, \mathrm{C}_n, \mathrm{D}_{n/2}, \quad \text{or } \mathrm{D}_{n/2}^2 \tag{A16}$$

according to whether the point corresponds to $(1,j)$ ($j = 1,2,3$ or 4). The critical point $(\mathbf{u}_c^0, f_c^0)$ is generically a limit point if the associated representation is (1, 1) and a simple, symmetric (pitchfork) bifurcation point otherwise.

For a double critical point related to a two-dimensional irreducible representation $(2,j)$, we note that

$$\Sigma(\alpha_1\boldsymbol{\xi}_1 + \alpha_2\boldsymbol{\xi}_2) = \Sigma(\beta_1\boldsymbol{\eta}_1 + \beta_2\boldsymbol{\eta}_2) = \mathrm{C}_m$$

for general coefficients $\alpha_i$ and $\beta_i$ $(i = 1, 2)$, where $m$ is the greatest common divisor of $n$ and $j$. Although vectors $\boldsymbol{\xi}_i$ and $\boldsymbol{\eta}_i$ $(i = 1, 2)$ in general are $C_m$-invariant, one can elaborately choose them to satisfy

$$\Sigma(\boldsymbol{\xi}_1) = \Sigma(\boldsymbol{\eta}_1) = D_m^1.$$

The space $X = \mathbf{R}^N$ of $\mathbf{w}$ is decomposed into mutually orthogonal subspaces of $X$ compatibly with the framework of the irreducible representations in eqn (A13), by means of the so-called isotypic (standard) decomposition, that is,

$$X = \bigoplus_{\mu \in R(D_n)} X^\mu, \tag{A17}$$

where $X^\mu$ are mutually orthogonal subspaces of $X$ associated with the irreducible representation $\mu = (\delta, j)$ and the symbol $\oplus$ expresses the direct sum.

### *A.4. Simple bifurcation point*

Asymptotic formulas for simple bifurcation points of a $D_n$-invariant system are derived here, as a refinement of Ikeda et al. (1997a, b) in view of group symmetry.

Suppose that the critical point $(\mathbf{u}_c^0, f_c^0)$ of a perfect $D_n$-symmetric system is a simple bifurcation point, with which a nonunit one-dimensional irreducible representation, $(1, j)$ with $j = 2$, 3, or 4 is associated. We may grasp the essential nature of eqn (A9) with eqn (A10) $(M = 1)$ by expanding it into a power series involving appropriate number of terms

$$\hat{F}(w, \tilde{f}, \varepsilon) \equiv \sum_{i=0} \sum_{j=0} \sum_{k=0} A_{ijk} w^i \tilde{f}^j \varepsilon^k = 0, \tag{A18}$$

where

$$A_{ijk} = A_{ijk}(\mathbf{d}) = \frac{1}{i!j!k!} \frac{\partial \hat{F}^{i+j+k}}{\partial w^i \, \partial \tilde{f}^j \, \partial \varepsilon^k} \bigg|_{(w, \tilde{f}, \varepsilon) = (0,0,0)}.$$

Since $(w, \tilde{f}, \varepsilon) = (0, 0, 0)$ corresponds to a critical point of the perfect system,

$$A_{000} = A_{100} = 0 \tag{A19}$$

must be satisfied.

Under the natural assumption that the group representation $S(g)$ is not disjoint from the nonunit irreducible representation $(1, j)$, the condition (A12) for $D_n$-equivariance of the bifurcation eqn (A10) may be replaced approximately by

$$T^{(1,j)}(g) \hat{F}(w, \tilde{f}, \varepsilon) = \hat{F}(T^{(1,j)}(g) w, \tilde{f}, T^{(1,j)}(g) \varepsilon), \quad g \in G. \tag{A20}$$

By the definition of $T^{(1,j)}(g)$ in eqn (A14), the symmetry condition in eqn (A20) reduces to:

$$-\hat{F}(w, \tilde{f}, \varepsilon) = \hat{F}(-w, \tilde{f}, -\varepsilon). \tag{A21}$$

This equation denotes that $\hat{F}(w, \tilde{f}, \varepsilon)$ is an odd function in $w$ and $\varepsilon$.

The condition for the criticality (A19) and that for the symmetry (A21) restricts the form of eqn (A18) to

$$\hat{F}(w,\tilde{f},\varepsilon) = A_{110}w\tilde{f}+A_{300}w^3+A_{001}\varepsilon+\text{h.o.t.} = 0. \tag{A22}$$

This coincides with the bifurcation eqn (4) in Section 2.2.

Next we consider the symmetry of the observed displacement $u_{i^*}$. Suppose $u_{i^*}$ has $D_n$-symmetry, i.e., that the $i^*$th unit vector $\mathbf{e}_{i^*}$ is invariant under the action of $D_n$. On the other hand, the critical eigenvector $\boldsymbol{\eta}_1$ corresponds to a nonunit one-dimensional irreducible representation. This implies that $\eta_{i^*1} = 0$ in the expression (A6). This is the group-theoretic explanation for the second case of the categorization in eqn (14).

### *A.5. Double bifurcation point*

We turn to a double bifurcation point of a $D_n$-invariant system.

#### *A.5.1. Symmetry in bifurcation equation*

Suppose that the critical point $(\mathbf{u}_c^0, f_c^0)$ of a perfect $D_n$-symmetric system is a group-theoretic double point, and let the two-dimensional irreducible representation $(2,j)$ with some $j$ of $D_n$ be associated with the kernel of $J^0 = J(\mathbf{u}_c^0, f_c^0, \mathbf{v}^0)$, which is spanned by $\boldsymbol{\eta}_1$ and $\boldsymbol{\eta}_2$. The vectors in the kernel space are invariant under $C_m$ (where $m$ is the greatest common divisor of $n$ and $j$). Note that $\hat{n} = n/m \geqslant 3$. We follow a standard technique (cf Sattinger, 1979; Golubitsky et al., 1988) to deal with a $D_n$-equivariant bifurcation equation.

We adopt complex coordinates $(z,\bar{z})$ instead of $(w_1,w_2)$ for the kernel space, i.e., $z = w_1+\mathrm{i}w_2$ and $\bar{z} = w_1-\mathrm{i}w_2$, and put

$$F(z,\bar{z},\tilde{f},\mathbf{v}) = \tilde{F}_1(w_1,w_2,\tilde{f},\mathbf{v})+\mathrm{i}\tilde{F}_2(w_1,w_2,\tilde{f},\mathbf{v}). \tag{A23}$$

The reduced eqns (A9) are equivalent to

$$F(z,\bar{z},\tilde{f},\mathbf{v}) = \overline{F(z,\bar{z},\tilde{f},\mathbf{v})} = 0, \tag{A24}$$

whereas the other eqn (A11) to

$$\left|\frac{\partial F}{\partial z}\right|^2-\left|\frac{\partial F}{\partial \bar{z}}\right|^2 = 0. \tag{A25}$$

With reference to the generic argument for $D_n$ (cf, Ikeda et al., 1991), the explicit form of $F$ is to be expressed as:

$$F = -\tilde{f}z-z^2\bar{z}+\sum_{2\leqslant q\leqslant \hat{n}/2-1} c_q z^{q+1}\bar{z}^q+b\bar{z}^{\hat{b}-1}+a\varepsilon, \tag{A26}$$

where $b$ and $c_q$ are real constants. With the use of the polar coordinates

$$z = r\exp(\mathrm{i}\theta), \quad \bar{z} = r\exp(-\mathrm{i}\theta), \quad a = |a|\exp(\mathrm{i}\psi),$$

in eqn (A26), eqn (A24) reduces to

$$r\tilde{f} = -r^3 + \sum_{2 \leqslant q \leqslant \hat{n}/2-1} c_q r^{2q+1} + br^{\hat{n}-1}\cos(\hat{n}\theta) + |a|\varepsilon\cos(\theta-\psi), \tag{A27}$$

$$br^{\hat{n}-1}\sin(\hat{n}\theta) + |a|\varepsilon\sin(\theta-\psi) = 0. \tag{A28}$$

The asymptotic expression of the bifurcation equation, accordingly, is dependent on the value of the index $\hat{n} = n/m$.

When $\hat{n} \geqslant 5$, it follows from eqns (A25) and (A26) that the critical point on the main path of an imperfect system is given by

$$\tilde{f} \sim \frac{-3|a|^{2/3}}{4^{1/3}}\varepsilon^{2/3}, \quad z \sim \frac{a}{2^{1/3}|a|^{2/3}}\varepsilon^{1/3}.$$

Combining these expressions with eqn (A28) we see that

$$r \sim \frac{|a|^{1/3}}{2^{1/3}}\varepsilon^{1/3}, \quad \theta-\psi = O(\varepsilon^{\frac{\hat{n}-4}{3}}).$$

Therefore, we can approximate eqn (A27) by

$$r\tilde{f} + r^3 - |a|\varepsilon = 0. \tag{A29}$$

It should be emphasized here that the bifurcation eqn (A29) for the double point with $\hat{n} \geqslant 5$ is of the same form as eqn (A22) for the simple symmetric bifurcation point.

When $\hat{n} = 3$ or 4, eqn (A27) becomes

$$\begin{cases} r\tilde{f} = br^2\cos(3\theta) + |a|\varepsilon\cos(\theta-\psi) & \text{if } \hat{n} = 3, \\ r\tilde{f} = -r^3 + br^3\cos(4\theta) + |a|\varepsilon\cos(\theta-\psi) & \text{if } \hat{n} = 4. \end{cases} \tag{A30}$$

*A.5.2. Asymptotic laws*

Asymptotic laws for a $D_n$-invariant displacement component $u_{i^*}$ are derived for the group-theoretic double bifurcation point with $\hat{n} \geqslant 5$. We show below that if $u_{i^*}$ is invariant under the action of $D_n$, then $\tilde{u}_{i^*}$ (with a particular $i^*$) becomes:

$$\tilde{u}_{i^*} = R_{i^*}\tilde{f} + S_{i^*}r^2 + \text{h.o.t.},$$

where $R_{i^*}$ and $S_{i^*}$ are constants.

Let $\mathbf{w}^{(\delta,j)}$ denote the component of $\mathbf{w}$ corresponding to the subspace $X^{(\delta,j)}$ in the isotypic decomposition in eqn (A17). Denoting by $N^{(\delta,j)}$ the multiplicity of the irreducible representation $(\delta,j)$, we see that $\mathbf{w}^{(\delta,j)}$ is of dimension $\delta \cdot N^{(\delta,j)}$. The variables $w_1$ and $w_2$ in eqn (A23) can be identified with some components of $\mathbf{w}^{(2,j)}$.

We further assume that the observed variable $u_{i^*}$ represents a displacement that is invariant under the action of $D_n$. This assumption implies that

$$\tilde{u}_{i^*} \equiv u_{i^*} - (u_{i^*})_c^0 = \sum_{k=1}^{N^{(1,1)}} \eta_{i^*k}^{(1,1)} w_k^{(1,1)}, \tag{A31}$$

where $\boldsymbol{\eta}_k^{(1,1)}$ $(k=1,\ldots,N^{(1,1)})$ denote those eigenvectors among $\boldsymbol{\eta}_k$ $(k=1,\ldots,N)$ which are $\mathrm{D}_n$-invariant [and belonging to the subspace $X^{(1,1)}$ in the isotypic decomposition (A17)].

As we have seen already, the bifurcation equation reduces approximately to eqn (A29), that is,

$$r\tilde{f}+r^3-|a|\varepsilon=0,$$

with $r=\sqrt{w_1^2+w_2^2}$. The remaining eqns (A8) for $\mathbf{w}^{(1,1)}$ are evaluated to

$$\hat{F}_k(\mathbf{w},\tilde{f},\varepsilon)=e_k^{(1,1)}w_k^{(1,1)}+a_k^{(1,1)}\tilde{f}+b_k^{(1,1)}\varepsilon + c_k^{11}w_1^2+c_k^{12}w_1w_2+c_k^{22}w_2^2+\text{h.o.t.}=0,\quad k=1,\ldots,N^{(1,1)}, \tag{A32}$$

where $a_k^{(1,1)}$, $b_k^{(1,1)}$, $e_k^{(1,1)}$, $c_k^{11}$, $c_k^{12}$ and $c_k^{22}$ $(k=1,\ldots,N^{(1,1)})$ are some constants ($b_k^{(1,1)}$ depends on the imperfection mode $\mathbf{d}$).

The group-equivariance of the whole set of eqn (A2) with respect to $\mathrm{D}_n$ is inherited to eqns (A32). By eqns (A14) and (A15), the action of the elements $c(2\pi/n)$ and $\sigma$ of the dihedral group $\mathrm{D}_n$ on these equations and on the variables in the equations is expressed as below:

$$c(2\pi/n):\quad \begin{pmatrix}w_1\\w_2\end{pmatrix}\mapsto\begin{pmatrix}\cos(2\pi j/n) & -\sin(2\pi j/n)\\ \sin(2\pi j/n) & \cos(2\pi j/n)\end{pmatrix}\begin{pmatrix}w_1\\w_2\end{pmatrix},\quad \sigma:\quad \begin{pmatrix}w_1\\w_2\end{pmatrix}\mapsto\begin{pmatrix}w_1\\-w_2\end{pmatrix},$$

$$c(2\pi/n),\sigma:\quad \hat{F}_k\mapsto\hat{F}_k,\quad w_k^{(1,1)}\mapsto w_k^{(1,1)}.$$

By virtue of this, the coefficients in the remaining eqns (A32) must satisfy

$$c_k^{11}=c_k^{22}(\equiv C_k),\quad c_k^{12}=0.$$

Equation (A32), accordingly, takes the form of

$$\hat{F}_k(\mathbf{w},\tilde{f},\varepsilon)=e_k^{(1,1)}w_k^{(1,1)}+a_k^{(1,1)}\tilde{f}+b_k^{(1,1)}\varepsilon+C_kr^2+\text{h.o.t.}=0,\quad k=1,\ldots,N^{(1,1)}. \tag{A33}$$

By eqn (A33), the variable $w_k^{(1,1)}$ can be evaluated to

$$w_k^{(1,1)}=-\frac{1}{e_k^{(1,1)}}(a_k^{(1,1)}\tilde{f}+C_kr^2)+\text{h.o.t.}, \tag{A34}$$

where $b_k^{(1,1)}\varepsilon$ is not included in this equation as it turns out to be a higher order term. The substitution of eqn (A34) into eqn (A31) results in

$$\tilde{u}_{i^*}=R_{i^*}\tilde{f}+S_{i^*}r^2+\text{h.o.t.}, \tag{A35}$$

where

$$R_{i^*}=-\sum_{k=1}^{N^{(1,1)}}\frac{\eta_{i^*k}^{(1,1)}a_k^{(1,1)}}{e_k^{(1,1)}},\quad S_{i^*}=-\sum_{k=1}^{N^{(1,1)}}\frac{\eta_{i^*k}^{(1,1)}C_k}{e_k^{(1,1)}}.$$

Note that eqn (A35) is exactly of the same form as eqn (20) for a $\mathrm{D}_n$-invariant displacement of a simple, symmetric bifurcation point with $\eta_{i^*1}=0$. In addition, recall that the bifurcation eqn (A29) for the double points is of the same form as eqn (11) for a simple point. As a consequence of these, all the results presented in Section 2.3 for a simple point apply to the double point with $\hat{n}=n/m\geqslant 5$

as well. It should be emphasized here that when $u_{i*}$ is not $D_n$-invariant, these results are not applicable.

Finally, we mention the case of $\hat{n} = 3$ and $\hat{n} = 4$, for which the orders of the terms in the bifurcation eqn (A30) are evaluated to:

$$r = O(\varepsilon^{1/2}), \quad \tilde{f} = O(\varepsilon^{1/2}), \quad \sin(\theta - \psi) = O(1) \quad \text{for } \hat{n} = 3,$$

$$r = O(\varepsilon^{1/3}), \quad \tilde{f} = O(\varepsilon^{2/3}), \quad \sin(\theta - \psi) = O(1) \quad \text{for } \hat{n} = 4.$$

For this reason, the asymptotic curve expressed by eqn (A30) for $\hat{n} = 3$ or 4 is dependent on $\psi$, and hence on the imperfection mode vector **d** even when $\varepsilon$ is infinitesimal. As we have seen, for $\hat{n} = 3$ or 4, the bifurcation equation becomes far more complex than that for $\hat{n} \geqslant 5$ in eqn (A29), and, in turn, such pertinent power laws as those for $\hat{n} \geqslant 5$ are not applicable.

## References


Ben-Haim, Y., Elishakoff, I., 1990. Convex models of uncertainty in applied mechanics. Studies in Applied Mechanics 25. Elsevier, Amsterdam.

Buzano, E., Geymonat, G., Poston, T., 1985. Post-buckling behavior of a non-linearly hyperelastic thin rod with cross-section invariant under the dihedral group $D_n$. Archive for Rational Mechanics and Analysis 89, 307–388.

Fujii, H., Mimura, M., Nishiura, Y., 1982. A picture of the global bifurcation diagram in ecological interacting and diffusing systems. Physica D—Nonlinear Phenomena 5, 1–42.

Gatermann, K., 1993. Computation of bifurcation graphs. In: Exploiting symmetry in applied and numerical analysis. AMS Lectures in Applied Mathematics, ed. E. Allgower, K. Georg, and R. Miranda, pp. 187–201.

Golubitsky, M., Schaeffer, D.G., 1985. Singularities and Groups in Bifurcation Theory 1. Springer, New York.

Golubitsky, M., Stewart, I.N., 1986. Hopf bifurcation with dihedral group symmetry: coupled nonlinear oscillators. In: Contemporary Mathematics, ed. M. Golubitsky and J. Guckenheimer. Multiparameter bifurcation theory. 56. A.M.S., Providence.

Golubitsky, M., Stewart, I., Schaeffer, D.G., 1988. Singularities and Groups in Bifurcation Theory 2. Springer, New York.

Healey, T.J., 1988. A group theoretic approach to computational bifurcation problems with symmetry. Computer Methods Applied Mechanics Engng 67, 257–295.

Hill, R., Hutchinson, J.W., 1975. Bifurcation phenomena in the plane tension test. Journal of the Mechanics and Physics of Solids 23, 239–264.

Hutchinson, J.W., Miles, J.P., 1974. Bifurcation analysis of the onset of necking in an elastic/plastic cylinder under uniaxial tension. Journal of the Mechanics and Physics of Solids 22, 61–71.

Ikeda, K., Goto, S., 1993. Imperfection sensitivity for size effect of granular materials. Soil Foundations 33 (2), 157–170.

Ikeda, K., Murota, K., 1993. Statistics of normally distributed initial imperfections. International Journal of Solids and Structures 30 (18), 2445–2467.

Ikeda, K., Murota, K., 1996. Bifurcation as sources of uncertainty in soil shearing behavior. Soils Foundations 36 (1), 73–84.

Ikeda, K., Murota, K., 1997. Recursive bifurcation as sources of complexity in soil shearing behavior. Soils Foundations 37 (3), 17–29.

Ikeda, K., Chida, T., Yanagisawa, E., 1997a. Imperfection sensitive strength variation of soil specimens. Journal of the Mechanics and Physics of Solids 45 (2), 293–315.

Ikeda, K., Murota, K., Fujii, H., 1991. Bifurcation hierarchy of symmetric structures. International Journal of Solids and Structures 27 (12), 1151–1573.

Ikeda, K., Murota, K., Yamakawa, Y., Yanagisawa, E., 1997b. Mode switching and recursive bifurcation in granular materials. Journal of the Mechanics and Physics of Solids 45 (11–12), 1929–1953.

Koiter, W.T., 1945. On the stability of elastic equilibrium. Dissertation. Delft, Holl, (English translation : NASA Tech. Trans. F10 : 833, 1967).

Murota, K., Ikeda, K., 1991. Critical imperfection of symmetric structures. SIAM Journal of Applied Mathematics 51 (5), 1222–1254.

Murota, K., Ikeda, K., 1992. On random imperfection for structures of regular-polygonal symmetry. SIAM Journal of Applied Mathematics 52 (6), 1780–1803.

Nakazawa, M., Ikeda, K., Wachi, S., Kuranishi, S., 1996. Numerical identification of secondary buckling phenomena of elastic rectangular plate under pure bending. Structural Eng./Earthquake Eng., JSCE 13 (1), 29s–41s.

Rudnicki, J.W., Rice, J.R., 1975. Conditions for the localization of deformation in pressure-sensitive dilatant materials. Journal of the Mechanics and Physics of Solids 23, 239–264.

Ruelle, D., 1973. Bifurcations in the presence of a symmetry group. Archives for Rational Mechanics and Analysis 51, 136–152.

Sattinger, D.H., 1979. Group Theoretic Methods in Bifurcation Theory. Lecture Notes in Mathematics 762, Springer.

Thom, R., 1972. Stabilité Structurelle et Morphogénèse. Benjamin, New York.

Thompson, J.M.T., Hunt, G.W., 1973. A General Theory of Elastic Stability. John Wiley and Sons, New York.

Thompson, J.M.T., Hunt, G.W., 1984. Elastic Instability Phenomena. John Wiley and Sons, Chichester.

Vardoulakis, I., 1988. Stability and bifurcation in geomaterials. Numerical Methods Geomechanics. ed. Swoboda Balkema, pp. 155–168.

Ziegler, H., 1968. Principles of Structural Stability. GinnBlaisdel, Lexington, MA.